DOCTORAL THESIS

Local absorbing boundary conditions for Korteweg-de-Vries-type equations

Zhang, Wei

Date of Award:
2014

Local Absorbing Boundary Conditions for Korteweg-de-Vries-Type Equations

ZHANG Wei

A thesis submitted in partial fulfillment of the requirements

for the degree of

Doctor of Philosophy

Principal Supervisor: Prof. WU Xiaonan

Hong Kong Baptist University

September 2014

Declaration

I hereby declare that this thesis represents my own work which has been done after registration for the degree of PhD at Hong Kong Baptist University, and has not been previously included in a thesis or dissertation submitted to this or any other institution for a degree, diploma or other qualifications.

Signature: _____

Date: September 2014

Abstract

The physicists and mathematicians have put a lot of efforts in the numerical analysis of various types of partial differential equations on unbounded domain. The time-dependent partial differential equations(PDEs) also have a wide range of applications in physics, geography and many other interdisciplines. This thesis is concerned with the numerical solutions of such kind of partial differential equations on unbounded spatial domain, especially the Korteweg-de Vries(KdV) equations. Since it is unable to solve the problem directly due to its unboundedness, the common way to surpass such difficulty is to introduce proper conditions on the truncated artificial boundaries and to approximate the problem on a bounded domain, which is also known as the Absorbing Boundary Conditions(ABCs).

One of the main contributions of this thesis is to design accurate local absorbing boundary conditions for linearized KdV equations and to extend the method to nonlinear KdV equations on unbounded domain. Padé approximation is the main tool to approximate the cubic root in the construction of local absorbing boundary conditions(LABCs) for a linearized KdV equation on unbounded domain. Besides, we also introduce the continued fraction method in the approximation of cubic root. To avoid the high-order derivatives in the absorbing boundary conditions, a sequence of auxiliary variables are applied accordingly. Then the original problem on unbounded domain is reduced to an approximated initial boundary value(IBV) problem defined on a finite domain.

Based on previous work, we are able to extend the method to the design of efficient local absorbing boundary conditions for nonlinear KdV equations on unbounded domain. The unifying approach method is applied to this nonlinear case. The idea of the unifying approach method is to separate inward- and outward-going waves and to build suitable approximated linear operator with a "one-way operator". Then we unite the approximated linear operator with the nonlinear subproblem and propose boundary conditions for the nonlinear subproblem along the artificial boundaries. The numerical simulations are given to demonstrate the effectiveness and accuracy

of our local absorbing boundary conditions.

Keywords: Korteweg-de Vries equation; Local absorbing boundary conditions; Padé approximation; Continued fraction method; Unifying approach.

Acknowledgements

First and foremost, I want to take this opportunity to thank my supervisor, Prof. Wu Xiaonan, for the patient guidance, constant encouragement that he has provided throughout my time as his student. His profound knowledge in mathematics, modesty and prudence attitudes in research influence me a lot. This thesis could not have reached its present form, without his consistent guidance and illuminating advices. His professional quality and good habits in research, remarkable characteristics in behaviors, will benefit me for life. I also thank to my co-supervisor, Dr. Zeng Tieyong. The enthusiasm he has for his research is contagious and motivational for me during my Ph.D. pursuit.

I thank Dr. Li Hongwei for his generous help during my freshman year in getting into the field, and good collaboration in the next few years. I am also sincerely grateful to Mr. Yang Jiang and Dr. Zhang Jiwei for their selfless assistances and inspiring discussions in my study. I thank all the fellow students for their friendships. My dear roommates and friends have made my life in Hong Kong a memorable one. I thank them for all the precious moments.

I wish to thank Hong Kong Baptist University for providing quality courses and the whole person education. I am also greatly indebted to the teachers, secretaries and technicians at the Department of Mathematics for their continuous help.

Most of all, I wish to express my gratitude to my family, for their love and confidence in me all along.

Table of Contents

Declaration i

Abstract ii

Acknowledgements iv

Table of Contents v

List of Tables vii

List of Figures viii

Chapter 1 Introduction 1

1.1 Artificial Boundary Conditions 1

1.2 Korteweg-de Vries (KdV) equation 3

1.3 Thesis Outline 5

Chapter 2 Local absorbing boundary conditions for a linearized KdV equation 6

2.1 Introduction 6

2.2 Design of the local absorbing boundary conditions 8

2.3 Stability analysis 15

2.3.1 Approximation of $\mathcal{L}^{-1}\{\frac{1}{\widetilde{\lambda}_p(s)}\}$ 15

2.3.2 Stability 16

2.4 Full discretization 20

2.5 Numerical results 22

2.6 Concluding remarks 28

Chapter 3 Continued fraction local absorbing boundary conditions for linearized KdV equation **31**

3.1 Introduction 31

3.2 Governing equation 33

3.3 The continued fraction approximation 35

3.4 The local absorbing boundary conditions 38

3.5 Numerical results 40

Chapter 4 Local absorbing boundary conditions for nonlinear KdV equations **46**

4.1 Introduction 46

4.2 Design of the local absorbing boundary conditions for KdV equation 48

4.2.1 A review on the unifying approach to split ABCs 48

4.2.2 LABCs for nonlinear KdV equation 50

4.3 Numerical results 54

Chapter 5 Summary **58**

5.1 Summary of the thesis 58

5.2 Future research 60

Bibliography **61**

Curriculum Vitae **65**

List of Tables

2.1 $\tilde{L}_1$ error in approximating $\sqrt[3]{s}$ and $\sqrt[3]{s^2}$ in the finite interval $s = [0.2, 9.9]$. 13

2.2 L_2 error and convergence order for the time space at $T = 2$. 23

2.3 L_2 error and convergence order for the spatial space at $T = 2$. 24

2.4 L_2 error and convergence order for the spatial space at $T = 4$. 24

2.5 L_2 error and convergence order for the time space at $T = 7$. 26

3.1 L_2 error and convergence order for the time space at $T = 1$. 41

3.2 L_2 error and convergence order for the spatial space at $T = 1$. 41

List of Figures

2.1 Padé approximation against the exact solution of $\sqrt[3]{s}$ with $p = 5$. . . . 12

2.2 Error of Padé approximation to $\sqrt[3]{s}$ with different $p = 3, 5, 7, 9$. 13

2.3 Numerical approximations of $\mathcal{L}^{-1}\{\frac{1}{\lambda_p(s)}\}$ compared with exact $\mathcal{L}^{-1}\{\frac{1}{-\sqrt[3]{s}}\}$ for different p. 17

2.4 Numerical solutions compared with exact solutions at different times as the parameter $p = 7$. 25

2.5 Numerical errors in L_2 norm with different p for time $T = 7$. 26

2.6 Numerical errors in L_∞ norm with different p for time $T = 7$. 27

2.7 The energy of the wave remaining in the bounded domain. 27

2.8 Numerical solutions compared with exact solutions at different times as the parameter $p = 9$. 29

2.9 The energy of the wave remaining in the bounded computational domain. 30

3.1 Continued fraction approximations of $\sqrt[3]{s}$ and corresponding error at different $p = 8, 16$. 37

3.2 Numerical solutions compared with exact solutions at different times as the parameter $p = 7$. 42

3.3 Numerical solutions compared with exact solutions at $T = 8$ with parameter $p = 5$. 42

3.4 Numerical errors in L_2 norm with different p for time $T = 2$. 43

3.5 Numerical errors in L_∞ norm with different p for time $T = 2$. 44

3.6 The energy of the wave remaining in the bounded domain $[-6, 6]$ with different parameter $p = 5$ and $p = 10$. 45

4.1 Numerical solutions compared with exact solutions at different times with single parameter. 56

4.2 Numerical errors compared with exact solutions at different times with single parameter. 57

Chapter 1

Introduction

1.1 Artificial Boundary Conditions

Many physical and industrial problems can be raised up as partial differential equations(PDEs) on unbounded domain, which includes water wave propagation, electromagnetics, acoustics, seismology and etc.. One of the difficulties to such problems is the unboundedness of calculation domain. Many researchers devote themselves to solve the problem of unbounded issue: the perfectly matched layer(PML) proposed by Berenger in 1994 [47] and the infinite element or boundary element method [48]. To cope with the difficulty brought by unboundedness of the defined domain, one of the most popular approaches is to cut off a finite computational domain from the unbounded domain and introduce the artificial boundary conditions, or the finite element methods.

In general, the artificial boundary conditions can be categorized into two main classes: explicit and implicit. The explicit artificial boundary conditions include: global ABCs (also called exact ABCs or non-reflecting boundary conditions), local ABCs and discrete ABCs [4]. The global artificial boundary conditions usually consist of the integrals of both function of interest and its derivatives, and can be well coupled with the finite element method. Hence, it is a common choice to use the global ABCs to find numerical solutions for elliptic PDEs on unbounded domain. The global ABCs guarantee the accuracy, at the same time, they demand a lot of computational cost. It often requires the historical data from the beginning to the computing time point, especially for some problems containing evolutions. When encountering long

time computation, people try to find the fast evaluation method in compensation for large computational demanding. On the other hand, the local artificial boundary conditions, generally given by equations including the function of interest and its derivatives, have been widely used in solving linear and nonlinear wave equations. The local ABCs are local in both space and time, which are computationally efficient and tractable. The local absorbing boundary is often regarded as an approximation to the exact absorbing boundary to the same problem. Nevertheless, high accuracy requirement in the local ABCs commonly introduces high order derivatives of the unknown function, which brings new difficulties to numerical implementation. The appropriate ABCs should not only be easy to be implemented, but also simulate the perfect absorption of waves leaving the computational domain through the artificial boundaries. The implicit ABCs are often in the form of an implicit integral equation that consists of the function of interest and its derivatives on the artificial boundaries. In most cases, the implicit ABCs are coming from the coupling equations of boundary element method and finite element method. The most outstanding advantage of the implicit ABCs is that they do not have special restrictions on the shape of artificial boundaries.

The local ABCs were proposed by Lindman [6] and made famous by Engquist and Majda [7]. They proposed the perfectly local absorbing boundary conditions for general classes of linear wave equations. However, it is limited by the difficulties posed in applying the high-order derivatives in the practical computations. Scientists contributed a lot on Laplace equations, Helmholtz-type equations in early years. The study of artificial boundary conditions has reached a fast developing stage in 1990s. The study field expanded greatly to many crucial partial differential equations and systems of PDEs that were involved in lots of physical applications. For instance, the exact ABCs were obtained for the system of 2-D and 3-D Navier equations, the system of Stokes equations and the system of Oseen equations. Moreover, mathemnaticians fully designed the perfectly absorbing boundary conditions for the acoustic waves

equation, Klein-Gordon equations, Schrödinger equations. In recent few years, there have been some new progress on the local ABCs for PDEs on unbounded domain. Hagstrom *et al.* [8, 9, 10, 11, 12] constructed high-order local absorbing boundary conditions for time-dependent waves by introducing special auxiliary variables. Guddati [15] constructed a new arbitrary high-order ABCs based on continued fraction approximation. Wu and Zhang [16] constructed the high-order local ABCs for heat equation and proved the stability of the coupled system. Zhang *et al.* [17, 18] constructed the local ABCs for the nonlinear Schrödinger equation on unbounded domain by applying the operator splitting method. Using the designed local ABCs, Brunner *et al.* [19, 20] studied the numerical solution of blow-up problems for semilinear parabolic equation on unbounded domain. Arnold *et al.* [21] proposed the discrete transparent boundary conditions for the time-dependent Schrödinger equation on a circular domain. Daalen and coworkers [22, 23] derived the radiation boundary conditions for wave equations by variational principles and conservation laws. The radiation boundary conditions are applicable to nonlinear and dispersive systems, and the reduced problem by the conditions is well-posed. For more works about the local ABCs and high-order local ABCs of PDEs on unbounded domains we refer to [24, 29, 26, 30, 31] and the review [32].

1.2 Korteweg-de Vries (KdV) equation

The governing equation of the Korteweg-de Vries equation is given as

$$u_t + u_{xxx} \pm 6uu_x = 0.$$

The dynamics of solitary water wave movement in a narrow channel is described by the Korteweg-de Vries (KdV) equation, which was initially appeared in Joseph Boussinesq's work in 1877 [39]. In fact, the phenomenons was firstly observed by John Scott Russell, a Scottish engineer, in the Edinburgh-Glasgow canal around mid-19th century. Later on Russell reproduced the motion of the water wave and established

detailed observation reports in a series of experiments in his home. In 1895, Diederik Korteweg and Gustav de Vries re-studied the equation in "On the Change of Form of Long Waves Advancing in a Rectangular Canal, and on a New Type of Long Stationary Waves" [38], and on the other side, demonstrated Russell's observation mathematically. Korteweg and de Vries also found the solitary wave solutions to the KdV equation that decay rapidly. Though Korteweg and de Vries's work was under-evaluated at that time and until 70 years later, Zabusky and Kruskal (1965) arrived at the Korteweg-de Vries equation unexpectedly during their study of the Fermi-Pasta-Ulam(FPU) equation. Korteweg and de Vries's work which had been neglected was renewed emphasis.

The KdV equation is nonlinear, dispersive and non dissipative. An important solution to this equation is called soliton, which was coined by Zabusky and Kruskal. Despite the nonlinearity of the solitary wave solutions, Zabusky and Kruskal found that the behavior of solitons was very similar to the superposition principle [40]. That is, the solitary waves preserve their velocity and shape when one passes through the other. Generally, the propagation speed of solitary waves is proportional to their amplitude.

In the following years, scientists carried forward theoretical work. The theory of the inverse scattering transform method enables us to obtain general solutions of some kinds of canonical nonlinear equations analytically. It is a very convenient and useful tool for solving the Cauchy problem for nonlinear evolution equations. The inverse scattering transform method maps the coefficient functions of a linear differential operator to a set of "scattering data". In 1967, Gardner, Greene, Kruskal and Miura firstly introduced the inverse scattering transform method and showed that the KdV equation was integrable [41]. The method also helped develop the analytic solution of KdV equation. Later in 1968, Miura *et al.* wrote a series of articles on Korteweg-de Vries equation and its generalizations, announcing the discovery of nine conservation laws and the tenth [43, 42]. The ground-breaking work done by these scientists

helped lay the foundation to the soliton theory and led to subsequent discoveries. Meanwhile, many different variations of the KdV equations, such as the generalized KdV equation, the modified KdV equation and the linearized KdV equation, are also been studied. The KdV equation plays an important role in various areas of physical applications, such as magneto hydrodynamics waves in warm plasma [53], acoustic waves in an inharmonic crystal [49]. The linearized KdV equation has been used to describe physical models which possess soliton structures in the shallow water for fairly long waves [1, 2, 3].

1.3 Thesis Outline

This thesis will emphasize on constructing different local absorbing boundary conditions for solving the linearized KdV equation and the KdV equation.

In Chapter 2, we first present a way of constructing local ABCs, with Padé approximation, to the linearized Korteweg-de Vries equation.

In Chapter 3, we adopt another approach with continued fraction approximation, to design the local ABCs for linearized Korteweg-de Vries equation. Due to the explicit clean form of continued fraction approximation, then we are able to extend the method to the nonlinear KdV equations.

In Chapter 4, based on the work in previous chapters, we arrive at the nonlinear KdV equations. In this chapter, according to the LABCs with continued fraction approximation given in the previous chapter, we construct local absorbing boundary conditions for nonlinear KdV equations using unifying approach.

Finally, conclusions and future work is elaborated in the last chapter.

Chapter 2

Local absorbing boundary conditions for a linearized KdV equation

2.1 Introduction

The Kortweg-de Vries (KdV) equation is a nonlinear partial differential equations (PDEs), which was originally used to describe the propagation of solitary wave on the water surface. Due to the presence of soliton solutions, this equation has attracted attention of mathematicians and physicists. The KdV equation arises in various areas of physical applications, such as magneto hydrodynamics waves in warm plasma, acoustic waves in an inharmonic crystal. The linearized KdV equation has been used to describe physical models which possess soliton structures in the shallow water for fairly long waves [1, 2, 3]. This chapter is devoted to studying the numerical solution of a linearized KdV equation on unbounded domain with Padé approximated local ABC's.

The initial value problem of a linearized KdV equation is given by the following form

$$u_t + u_{xxx} = h(x,t),\ x \in \mathbb{R}, t \in [0,T], \tag{2.1}$$

$$u(x,0) = u_0(x),\quad x \in \mathbb{R}, \tag{2.2}$$

$$u \to 0, \qquad |x| \to +\infty, \tag{2.3}$$

where $h(x,t)$ and $u_0(x)$ denote source term and initial condition with compactly supports, i.e., there is a finite interval $[a,b]$ such that Supp$\{h(x,t) \subset [a,b] \times [0,T]\}$, and Supp$\{u_0(x) \subset [a,b]\}$. To cope with the difficulty brought by unboundedness of the defined domain, one of the most popular approaches is to cut off a finite computational domain from the unbounded domain and apply the so-called absorbing boundary conditions (ABCs) on the artificial boundaries. The appropriate ABCs should not only be easy to implement, but also imitate the perfect absorption of waves leaving the computational domain through the artificial boundaries.

The Padé approximation was introduced by Engquist and Majda to designed the highly absorbing local boundary conditions for wave equations [7]. They approximated a square root with the Padé approximation. Due to the simple and straightforward form brought by the approximation, Padé approximation is convenient and efficient in the construction of local ABCs for some PDEs. Zheng *et al.* [3] constructed the global (exact) absorbing boundary conditions for a linearized KdV equation. The authors separated the unbounded domain of an initial value problem into three subproblems and performed Laplace transformation to two new subproblems on unbounded domain. After solving the two subproblems in the frequency domain, the global ABCs for linearized KdV equation are derived. Since the global ABCs try to simulate the effect of the exterior in an exact sense and are fully coupled in space and time, they are very expensive for practical computations. Zheng *et al.* developed a fast evaluation method to reduce the computational cost of convolution operations involved in the global ABCs. Based on the ABCs proposed by Fokas [46] for a modified KdV equation, Zheng [5] set up a kind of non-reflecting boundary conditions(NRBC) which are suitable for numerical purposes and the discretization of the non-reflecting boundary conditions is studied in detail. When the NRBCs are imposed on the artificial boundary points, a reduced problem that has the same solution as the original exact NRBCs one, is derived on a finite domain. Zheng introduced the dual -Petrov-Galerkin spectral method for the discretization of the reduced

problem with NRBCs on bounded axis. However, Zheng did not manage to extend the NRBCs to nonlinear problem.

The organization of the chapter is as follows. In Sec. 2.2, we construct the local ABCs for linearized KdV equation by using the Padé approximation, and obtain an initial boundary value problem (IBVP) on a bounded computational domain. In Sec. 2.3, we show that the reduced initial boundary value problem is stable in the limiting case. A finite difference scheme is presented to solve the reduced IBVP in Sec. 2.4. In Sec. 2.5, numerical results are given to demonstrate the effectiveness and stability of the proposed method.

2.2 Design of the local absorbing boundary conditions

In this section we are devoted to the derivation of highly accurate local ABCs for the linearized KdV equation (2.1)-(2.3) by applying Padé approximation. The studies concerning the absorbing boundary conditions by rational approximation can be found in the works Bruneau and coworkers [33], Szeftel [34, 35] and others [36].

Following [3], we introduce the following artificial boundaries:

$$\begin{aligned} \Omega_a &= \{(x,t)|x=a,\ 0\le t\le T\}, \\ \Omega_b &= \{(x,t)|x=b,\ 0\le t\le T\}. \end{aligned}$$

The unbounded domain $\mathbb{R}^1\times[0,T]$ are divided into three parts by the artificial boundaries Ω_a and Ω_b, namely, the bounded domain $D_i=[a,b]\times[0,T]$, and the unbounded parts $D_L=(-\infty,a]\times[0,T]$ and $D_R=[b,+\infty)\times[0,T]$. In order to study the numerical solution of linearized KdV equation, we must find the boundary conditions on the artificial boundaries Ω_a and Ω_b, to reduce the original problem into an initial boundary value problem on the finite computational domain.

Next, we consider the following three problems:

$$\begin{aligned} u_t + u_{xxx} &= 0, \qquad x > b, 0 \le t \le T, && (2.4)\\ u(x,t)|_{x=b} &= u(b,t),\ 0 \le t \le T, && (2.5)\\ u(x,0) &= 0, \qquad x > b, && (2.6)\\ u &\to 0, \qquad x \to +\infty, && (2.7) \end{aligned}$$

and

$$\begin{aligned} u_t + u_{xxx} &= 0, \qquad x \in [a,b], 0 \le t \le T, && (2.8)\\ u(x,t)|_{x=a} &= u(a,t),\ 0 \le t \le T, && (2.9)\\ u(x,t)|_{x=b} &= u(b,t),\ 0 \le t \le T, && (2.10)\\ u(x,0) &= u_0(x,0),\ 0 \le t \le T, && (2.11)\\ & && (2.12) \end{aligned}$$

and

$$\begin{aligned} u_t + u_{xxx} &= 0, \qquad x < a, 0 \le t \le T, && (2.13)\\ u(x,t)|_{x=a} &= u(a,t),\ 0 \le t \le T, && (2.14)\\ u(x,0) &= 0, \qquad x < a, && (2.15)\\ u &\to 0, \qquad x \to -\infty. && (2.16) \end{aligned}$$

Since $u(b,t)$ and $u(a,t)$ are not known, both problems are not complete, and can not be solved. We can solve the problems (2.4)-(2.7) and (2.13)-(2.16), if the functions $u(b,t)$ and $u(a,t)$ are given.

Applying the Laplace transformation to equations (2.4)-(2.7), we obtain

$$s\hat{u} + \hat{u}_{xxx} = 0, \tag{2.17}$$

where

$$\hat{u}(x,s) = \int_0^{+\infty} e^{-st} u(x,t)dt,\ s \in \mathbb{C},\ \mathrm{Re}(s) > 0.$$

The general solution of equation (2.17) can be found as

$$\hat{u}(x,s) = c_1(s)e^{\lambda_1(s)x} + c_2(s)e^{\lambda_2(s)x} + c_3(s)e^{\lambda_3(s)x}, \tag{2.18}$$

where

$$\lambda_1(s) = -\sqrt[3]{s}, \lambda_2(s) = -\sqrt[3]{s}\omega, \lambda_3(s) = -\sqrt[3]{s}\omega^2, \omega = e^{\frac{2\pi i}{3}}.$$

Notice that

$$\begin{aligned} &\mathrm{Re}\{\lambda_1(s)\} < 0, \mathrm{Re}\{\lambda_2(s)\} > 0, \\ &\mathrm{Re}\{\lambda_3(s)\} > 0, \quad \forall\ \mathrm{Re}\{s\} > 0. \end{aligned}$$

Therefore, we have $c_2(s) = 0$ and $c_3(s) = 0$ in equation (2.18), since $\hat{u}(x,s)$ vanishes as $x \to +\infty$. Similarly, we conclude $c_1(s) = 0$ from the problem (2.13)-(2.16). Thus, we have

$$\hat{u}(b,s) - \frac{1}{\lambda_1^2(s)}\hat{u}_{xx}(b,s) = 0, \tag{2.19}$$

$$\hat{u}_x(b,s) - \frac{1}{\lambda_1(s)}\hat{u}_{xx}(b,s) = 0, \tag{2.20}$$

$$\hat{u}(a,s) + \frac{1}{\lambda_1(s)}\hat{u}_x(a,s) + \frac{1}{\lambda_1^2(s)}\hat{u}_{xx}(a,s) = 0. \tag{2.21}$$

Applying inverse Laplace transform to equations (2.19)-(2.21), then we get the global absorbing boundary conditions. Unfortunately, it is difficult to implement the inverse Laplace transformation, since there involves expensive convolution operations. In order to overcome this disadvantage and obtain manageable boundary conditions, we apply the effective Padé approximate method. For calculation simplicity, we define the new approximation as following,

$$f(z) = (1-z)^\alpha = 1 - \sum_{i=1}^{\infty} \frac{b_i z}{1 - a_i z}.$$

Then, we consider Padé approximation of $\lambda_1(s) = -\sqrt[3]{s}$,

$$-\sqrt[3]{s} = -[1-(1-s)]^{\frac{1}{3}} = -1 + \sum_{i=1}^{\infty} \frac{b_i z}{1 - a_i z}, \tag{2.22}$$

where $z = 1-s$. By comparing coefficients of n-th order derivatives between Maclaurin series and Padé series, the coefficients a_i and b_i $(i = 1, 2, \cdots, p)$ can be determined uniquely by the following nonlinear system,

$$\sum_{i=1}^{2p} C_i z^i = -\sum_{i=1}^{p} \frac{b_i z}{1 - a_i z}. \tag{2.23}$$

Take derivative on both sides of equation (2.23) continuously and set $z = 0$ each time

$$\begin{aligned} C_1 &= -\sum_{i=1}^{p} b_i, \\ 2C_2 &= -2\sum_{i=1}^{p} a_i b_i, \\ &\vdots \\ (2p-1)!C_{2p} &= -(2p-1)!\sum_{i=1}^{p} a_i^{2p-1} b_i. \end{aligned}$$

Denote $d_i = a_i^p b_i$, we have the following nonlinear system. Thus a_i and b_i can be calculated.

$$\begin{aligned} b_1 + b_2 + \cdots + b_p &= -C_1, \\ a_1 b_1 + a_2 b_2 + \cdots + a_p b_p &= -C_2, \\ &\vdots \\ a_1^{p-1} b_1 + a_2^{p-1} b_2 + \cdots + a_p^{p-1} b_p &= -C_p, \\ d_1 + d_2 + \cdots + d_p &= -C_{p+1}, \\ a_1 d_1 + a_2 d_2 + \cdots + a_p d_p &= -C_{p+2}, \\ &\vdots \\ a_1^{p-1} d_1 + a_2^{p-1} d_2 + \cdots + a_p^{p-1} d_p &= -C_{2p}. \end{aligned}$$

Solving the above system, we obtain the coefficients a_i and b_i $(i = 1, 2, \cdots, p)$. $\lambda_1(s) = -\sqrt[3]{s}$ can be easily estimated by truncated p terms of the Padé series, namely,

$$\lambda_1(s) \approx \tilde{\lambda}_p(s) = -1 + \sum_{i=1}^{p} \frac{b_i(1-s)}{1 - a_i(1-s)}.$$

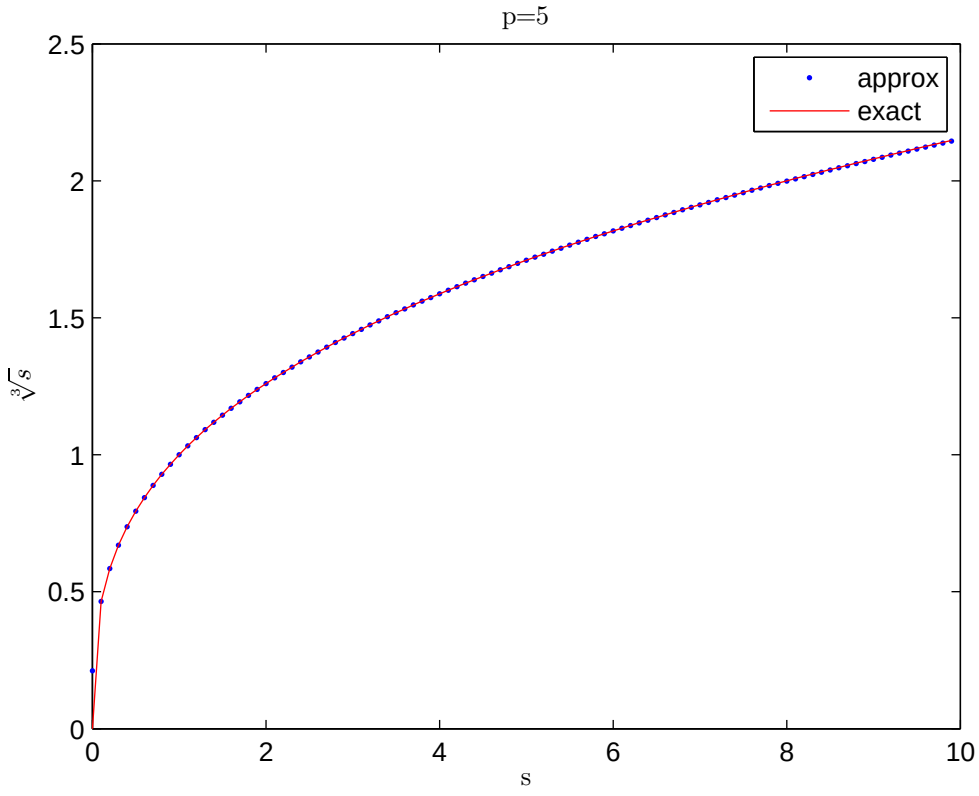

Figure 2.1: Padé approximation against the exact solution of $\sqrt[3]{s}$ with $p = 5$.

Fig. 2.1 shows the Padé approximation of $\sqrt[3]{s}$ when $p = 5$. Compare the approximate solution with the corresponding exact solution in this figure, one can observe that they are almost indistinguishable.

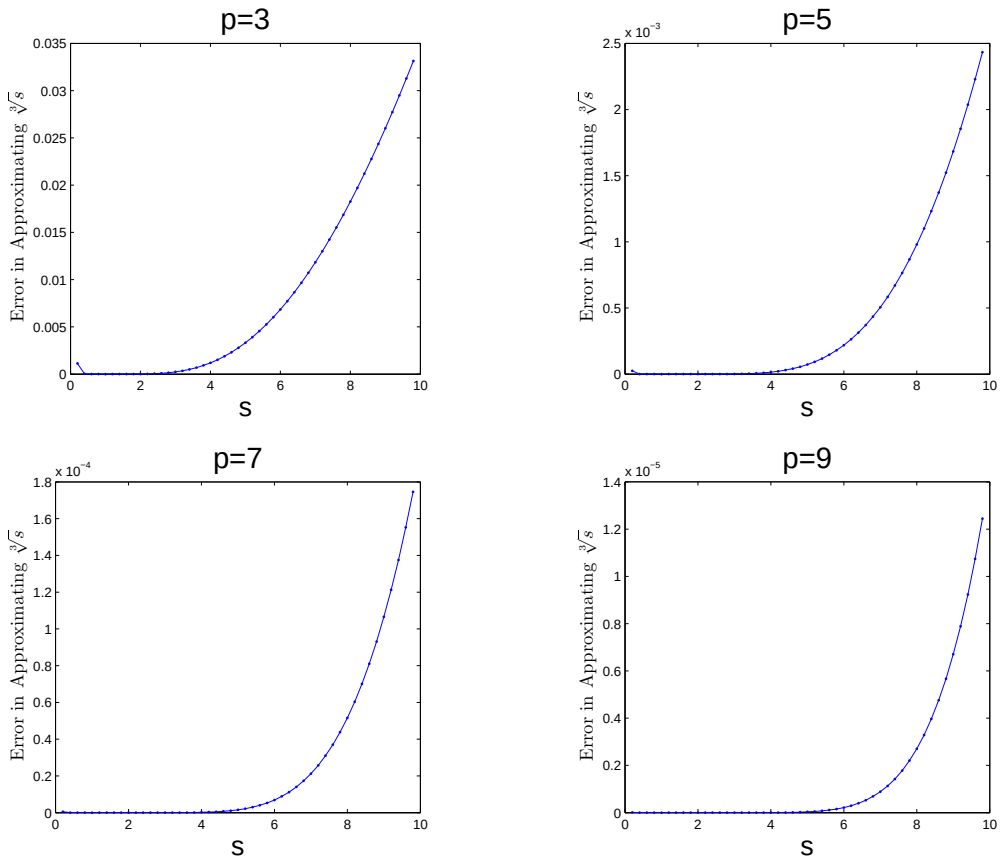

Figure 2.2: Error of Padé approximation to $\sqrt[3]{s}$ with different $p = 3, 5, 7, 9$.

Table 2.1: $\tilde{L}_1$ error in approximating $\sqrt[3]{s}$ and $\sqrt[3]{s^2}$ in the finite interval $s = [0.2, 9.9]$.

	$p = 3$	$p = 5$	$p = 7$	$p = 9$
$\sqrt[3]{s}$	8.356e-3	4.588e-4	2.657e-5	1.598e-6
$\sqrt[3]{s^2}$	1.970e-2	1.034e-3	5.887e-5	3.510e-6

Fig. 2.2 plots the error of exact value and the approximated value of $\sqrt[3]{s}$ with different p. Tab. 2.1 lists the $\tilde{L}_1$ error in approximating $\sqrt[3]{s}$ and $\sqrt[3]{s^2}$ in the interval

$s = [0.2, 9.9]$, which is defined by

$$\tilde{L}_1 = \frac{1}{K}\sum_{k=1}^{K} |\lambda_1^m(s_k) - \tilde{\lambda}_p^m(s_k)|, \ (m = 1, 2).$$

We can see that the error decreases as the parameter p grows. Numerical results indicate that when p is greater than 5, $\sqrt[3]{s}$ can be approximated by the Padé approximation very well.

Similarly, $\lambda_1^2(s) = (\sqrt[3]{s})^2$ can be estimated by using the same method, with the corresponding parameters A_i and B_i $(i = 1, 2, \cdots, p)$. Using Padé approximation to $\lambda_1^2(s)$ in equation (2.19), we have

$$\lambda_1^2(s) = \sqrt[3]{s^2} \approx \tilde{\lambda}_p^2(s) = 1 - \sum_{i=1}^{p} \frac{B_i(1-s)}{1 - A_i(1-s)}.$$

Let

$$\hat{g}_r = \frac{1}{\tilde{\lambda}_p^2(s)} \hat{u}_{xx}(b, t),$$

a system of equations is given as following

$$\begin{aligned} \hat{u} - \hat{g}_r &= 0, && (2.24)\\ \hat{g}_r - \sum_{i=1}^{p} B_i \hat{w}_i &= \hat{u}_{xx}, && (2.25)\\ \frac{1-s}{1 - A_i + A_i s}\hat{g}_r &= \hat{w}_i, i = 1, 2, \cdots, p. && (2.26) \end{aligned}$$

Applying inverse Laplace transform to equations (2.24)-(2.26), we obtain

$$\begin{aligned} u - g_r &= 0, && (2.27)\\ g_r - \sum_{i=1}^{p} B_i w_i &= u_{xx}, && (2.28)\\ (1 - A_i)w_i + A_i \frac{dw_i}{dt} &= g_r - \frac{dg_r}{dt}, i = 1, 2, \cdots, p. && (2.29) \end{aligned}$$

In a similar way, we assume $\hat{f}_r = -\frac{1}{\tilde{\lambda}_p(s)} \hat{u}_{xx}(b, t)$. Using Padé approximation to $\lambda_1(s)$ in equation (2.20), we get

$$\begin{aligned} \hat{u}_x + \hat{f}_r &= 0,\\ \hat{f}_r - \sum_{i=1}^{p} b_i \hat{v}_i &= \hat{u}_{xx},\\ \frac{1-s}{1 - a_i + a_i s}\hat{f}_r &= \hat{v}_i, i = 1, 2, \cdots, p. \end{aligned}$$

After performing the inverse Laplace transformation on above system,

$$\begin{aligned} u_x + f_r &= 0, && (2.30)\\ f_r - \sum_{i=1}^{p} b_i v_i &= u_{xx}, && (2.31)\\ (1-a_i)v_i + a_i\frac{dv_i}{dt} &= f_r - \frac{df_r}{dt}, i = 1, 2, \cdots, p. && (2.32) \end{aligned}$$

For equation (2.21), let

$$\hat{f}_l = -\frac{1}{\tilde{\lambda}_p(s)}\hat{u}_x(a,t) \text{ and } \hat{g}_l = \frac{1}{\tilde{\lambda}_p^2(s)}\hat{u}_{xx}(a,t).$$

A_i and a_i $(i = 1, 2, \cdots, p)$ are defined as before. Applying the inverse Laplace transformation, we have

$$\begin{aligned} u - f_l + g_l &= 0, && (2.33)\\ f_l - \sum_{i=1}^{p} b_i \bar{v}_i &= u_x, && (2.34)\\ g_l - \sum_{i=1}^{p} B_i \bar{w}_i &= u_{xx}, && (2.35)\\ (1-a_i)\bar{v}_i + a_i\frac{d\bar{v}_i}{dt} &= f_l - \frac{df_l}{dt}, && (2.36)\\ (1-A_i)\bar{w}_i + A_i\frac{d\bar{w}_i}{dt} &= g_l - \frac{dg_l}{dt}, && (2.37) \end{aligned}$$

where $i = 1, 2, \cdots, p$.

Coupling the local ABCs (2.27)-(2.37) with the linearized KdV equation, we have the reduced IBVP on the bounded computational domain.

2.3 Stability analysis

2.3.1 Approximation of $\mathcal{L}^{-1}\{\frac{1}{\tilde{\lambda}_p(s)}\}$

Before the analysis of the stability, we first review and introduce the relative lemma for Padé approximation. Despite the Padé expansion in equation (2.22), $\frac{1}{\tilde{\lambda}_p(s)}$ can

also be rewritten into a finite series of partial fractions as following,

$$\frac{1}{-1+\sum_{i=1}^{p}\frac{b_i(1-s)}{1-a_i(1-s)}} = \sum_i \frac{r_i}{s-q_i} + c,$$

where r_i, q_i and c are constants. The reason we are reforming this expansion equation is to pursue a better sight of view after performing the inverse Laplace transformation on $\frac{1}{\tilde{\lambda}_p(s)}$. Therefore, under such expansion, $\mathcal{L}^{-1}\{\frac{r_i}{s-q_i}\}$ can be easily found as $r_i e^{q_i t}$ and $\mathcal{L}^{-1}\{k\} = k\delta(t)$.

Due to the linearity of inverse Laplace operator, we have

$$\mathcal{L}^{-1}\{\frac{1}{\tilde{\lambda}_p(s)}\} = \sum_i r_i e^{q_i t} + k\delta(t).$$

Similarly, we can also find the inverse Laplace transformation for $\mathcal{L}^{-1}\{\frac{1}{\tilde{\lambda}_p^2(s)}\}$.

As seen in Fig. 2.3, the exact solution and partial fraction approximation of $\mathcal{L}^{-1}\{\frac{1}{-\sqrt[3]{s}}\}$ for different p is plotted. From this figure, we observe that the performance of the approximation is very well, and the numerical results suggest the following lemma:

Lemma 2.1. *Given that* $\lim_{p\to\infty} \tilde{\lambda}_p(s) = \lambda_1(s)$ *and* $\lim_{p\to\infty} \tilde{\lambda}_p^2(s) = \lambda_1^2(s)$*, for* $s \geq 0$*, it is reasonable to admit that*

$$h_1(t) := \lim_{p\to\infty} \mathcal{L}^{-1}\{\frac{1}{\tilde{\lambda}_p(s)}\} = \mathcal{L}^{-1}\{\frac{1}{\lambda_1(s)}\},$$

$$h_2(t) := \lim_{p\to\infty} \mathcal{L}^{-1}\{\frac{1}{\tilde{\lambda}_p^2(s)}\} = \mathcal{L}^{-1}\{\frac{1}{\lambda_1^2(s)}\},$$

$$|h_q(t)| \leq ct^d, \qquad d \in (-1, 0), \qquad q = 1, 2.$$

2.3.2 Stability

In order to analyze the stability of the reduced IBVP and state our main results, we define fractional integral operator I_α with $\alpha > 0$ as [37]

$$I_t^\alpha f(t) = \frac{1}{\Gamma(\alpha)} \int_0^t (t-\tau)^{\alpha-1} f(\tau) d\tau, \quad t > 0.$$

We have the following Lemmas:

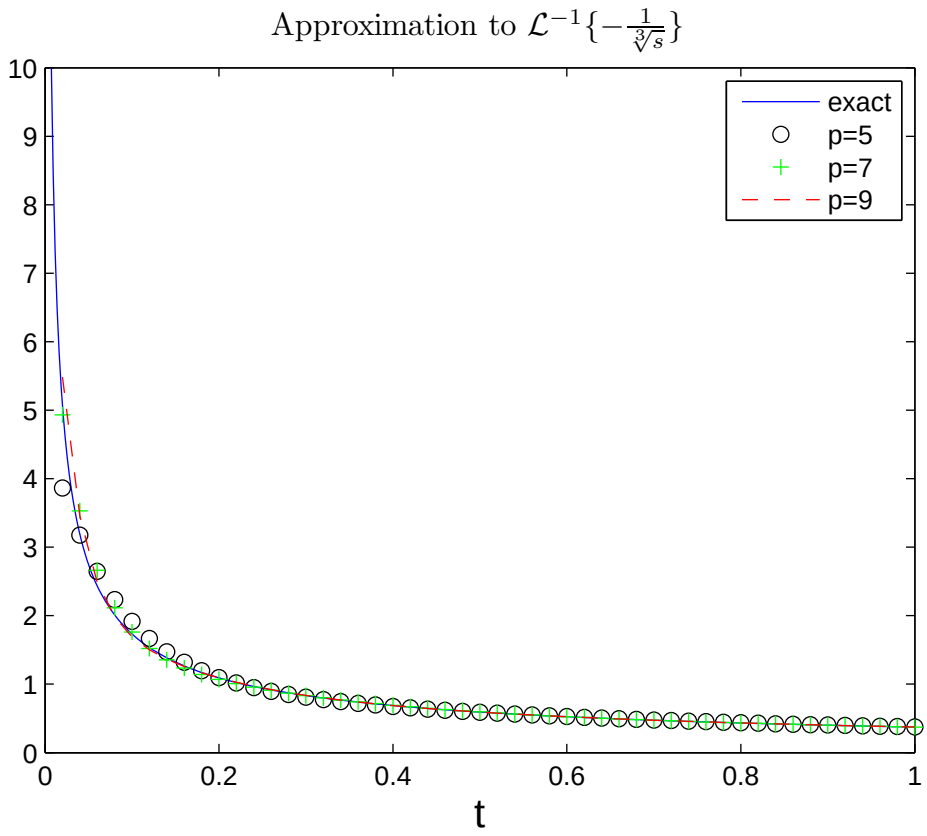

Figure 2.3: Numerical approximations of $\mathcal{L}^{-1}\{\frac{1}{\tilde{\lambda}_p(s)}\}$ compared with exact $\mathcal{L}^{-1}\{\frac{1}{-\sqrt[3]{s}}\}$ for different p.

Lemma 2.2. *Assume* $\lim_{p\to\infty}\mathcal{L}^{-1}\{\frac{1}{\tilde{\lambda}_p(s)}\}=\mathcal{L}^{-1}\{\frac{1}{\lambda_1(s)}\}$, *and* $\lim_{p\to\infty}\mathcal{L}^{-1}\{\frac{1}{\tilde{\lambda}_p^2(s)}\}=\mathcal{L}^{-1}\{\frac{1}{\lambda_1^2(s)}\}$. *Then for any bounded integrable function* f, *we have*

$$\lim_{p\to\infty}\mathcal{L}^{-1}\{\frac{1}{\tilde{\lambda}_p(s)}\hat{f}\}=-I_t^{\frac{1}{3}}f,$$

$$\lim_{p\to\infty}\mathcal{L}^{-1}\{\frac{1}{\tilde{\lambda}_p^2(s)}\hat{f}\}=I_t^{\frac{2}{3}}f.$$

Proof:

$$\lim_{p\to\infty}\mathcal{L}^{-1}\{\frac{1}{\tilde{\lambda}_p(s)}\hat{f}\}=\lim_{p\to\infty}(\mathcal{L}^{-1}\{\frac{1}{\tilde{\lambda}_p(s)}\}*f)(t)$$
$$=\lim_{p\to\infty}\int_0^t\mathcal{L}^{-1}\{\frac{1}{\tilde{\lambda}_p(s)}\}(t-\tau)f(\tau)d\tau.$$

By the Lebesgue's Dominated Convergence Theorem, we can interchange the limit and integration, i.e.,

$$\begin{aligned}\lim_{p\to\infty}\mathcal{L}^{-1}\{\frac{1}{\tilde{\lambda}_p(s)}\hat{f}\} &= \int_0^t\lim_{p\to\infty}\mathcal{L}^{-1}\{\frac{1}{\tilde{\lambda}_p(s)}\}(t-\tau)f(\tau)d\tau\\ &= \int_0^t\frac{1}{\lambda_1}(t-\tau)f(\tau)d\tau\\ &= -\frac{1}{\Gamma(\frac{1}{3})}\int_0^t(t-\tau)^{-\frac{2}{3}}f(\tau)d\tau\\ &= -I_t^{\frac{1}{3}}f.\end{aligned}$$

Likewise, $\lim_{p\to\infty}\mathcal{L}^{-1}\{\frac{1}{\tilde{\lambda}_p^2(s)}\hat{f}\}=I_t^{\frac{2}{3}}f$ can be proved. □

Lemma 2.3. *For any smooth functions* $f(t)$ *and* $g(t)$ *with* $f(0)=g(0)=0$, *it holds*

$$\begin{aligned}I_t^1[2fI_t^{\frac{2}{3}}f-(I_t^{\frac{1}{3}}f)^2] &\geq 0,\\ I_t^1[2(I_t^{\frac{1}{3}}g-I_t^{\frac{2}{3}}f)f-g^2] &\leq 0.\end{aligned}$$

The proof has been given in [3].

Theorem 2.1. *Given that* $\lim_{p\to\infty}\mathcal{L}^{-1}\{\frac{1}{\tilde{\lambda}_p(s)}\}=\mathcal{L}^{-1}\{\frac{1}{\lambda_1(s)}\}$, *and* $\lim_{p\to\infty}\mathcal{L}^{-1}\{\frac{1}{\tilde{\lambda}_p^2(s)}\}=\mathcal{L}^{-1}\{\frac{1}{\lambda_1^2(s)}\}$. *Let* u *be the solution of the linear KdV equation coupled with the absorbing boundary conditions (2.27)-(2.37) as* $p\to\infty$. *Then for any* $t>0$, *there exists a constant positive number* $c(t)$, *such that*

$$\int_a^b u^2(x,t)dx\leq c(t)\left[\int_a^b u_0^2(x)dx+\int_0^t\int_a^b h^2(x,\tau)dxd\tau\right]. \tag{2.38}$$

Proof: Multiplying equation (2.1) by $2u(x,t)$ on both sides and integrating with respect to x over $[a,b]$

$$\begin{aligned}
& \frac{d}{dt}\int_a^b u^2(x,t)dx \\
= & -2\int_a^b u(x,t)u_{xxx}(x,t)dx + \int_a^b 2h(x,t)u(x,t)dx \\
= & -2\left[u(x,t)u_{xx}(x,t)|_a^b - \int_a^b u_x(x,t)u_{xx}(x,t)dx\right] \\
& + \int_a^b 2h(x,t)u(x,t)dx \\
= & \ 2\left[u(a,t)u_{xx}(a,t) - \frac{1}{2}u_x^2(a,t)\right] \\
& -2\left[u(b,t)u_{xx}(b,t) - \frac{1}{2}u_x^2(b,t)\right] + \int_a^b 2h(x,t)u(x,t)dx \\
= & \ [2(f_l - g_l)u_{xx}(a,t) - u_x^2(a,t)] - [2g_r u_{xx}(b,t) - f_r^2] \\
& + \int_a^b 2h(x,t)u(x,t)dx.
\end{aligned}$$

Combining the absorbing boundary conditions (2.27), (2.30) and (2.33), take limit and integrate both sides of the above equation with respect to t, then

$$\begin{aligned}
& \int_a^b u^2(x,t)dx - \int_a^b u_0^2(x)dx \\
= & \lim_{p\to\infty}\int_0^t [(2(f_l - g_l)u_{xx}(a,\tau) - u_x^2(a,\tau)) \\
& -(2g_r u_{xx}(b,\tau) - f_r^2)]d\tau \\
& + \lim_{p\to\infty}\int_0^t\int_a^b 2h(x,\tau)u(x,\tau)dxd\tau \\
= & \int_0^t \left[\lim_{p\to\infty} 2(f_l - g_l)u_{xx}(a,\tau) - u_x^2(a,\tau)\right]d\tau \\
& - \int_0^t \left[\lim_{p\to\infty} 2g_r u_{xx}(b,\tau) - f_r^2\right]d\tau \\
& + \int_0^t\int_a^b 2h(x,\tau)u(x,\tau)dxd\tau.
\end{aligned}$$

Due to the Lemma 2.2, we have $\lim_{p\to\infty} f_l = I_t^{\frac{1}{3}}u_x(a,t)$, $\lim_{p\to\infty} g_l = I_t^{\frac{2}{3}}u_{xx}(a,t)$, $\lim_{p\to\infty} f_r =$

$I_t^{\frac{1}{3}} u_x(b,t)$ and $\lim_{p\to\infty} g_r = I_t^{\frac{2}{3}} u_{xx}(b,t)$. Therefore, with the conclusion of Lemma 2.3,

$$\begin{aligned}
&\int_a^b u^2(x,t)dx - \int_a^b u_0^2(x)dx \\
= \;& I_t^1[2(I_t^{\frac{1}{3}} u_x(a,t) - I_t^{\frac{2}{3}} u_{xx}(a,t))u_{xx}(a,t) - u_x^2(a,t)] \\
- \;& I_t^1[2u_{xx}(b,t)I_t^{\frac{2}{3}} u_{xx}(b,t) - (I_t^{\frac{1}{3}} u_x^2(b,t))] \\
+ \;& \int_0^t \int_a^b 2h(x,\tau)u(x,\tau)dxd\tau \\
\leq \;& \int_0^t \int_a^b 2h(x,\tau)u(x,\tau)dxd\tau \\
\leq \;& \int_0^t \int_a^b \left[h^2(x,\tau) + u^2(x,\tau)\right] dxd\tau
\end{aligned}$$

Hence, according to the Gronwall's inequality, we get

$$\begin{aligned}
\int_a^b u^2(x,t)dx \leq & \int_0^t \int_a^b u^2(x,\tau)dxd\tau \\
& + \int_0^t \int_a^b h^2(x,\tau)dxd\tau + \int_a^b u_0^2(x)dx.
\end{aligned}$$

This completes the proof. □

Remark: *Theorem 4 gives the stability as $p \to \infty$. However, p is usually small in the numerical approximation. Thus, further study is needed to investigate the stability for a fixed p.*

2.4 Full discretization

In this section, we discuss the discretized forms for the reduced IBVP on the bounded computational domain $[a,b]\times[0,T]$. We divide the computational domain by a set of lines parallel to the x-axis and t-axis to form a grid. For given two positive integers J and N, we get the spatial and temporal mesh sizes by defining $\Delta x = \frac{b-a}{J}$ and $\Delta t = \frac{T}{N}$. Thus, the uniform grid points can be written as $x_j = a + j\Delta x, (j = 0, 1, 2, \cdots, J)$ and $t_n = n\Delta t, (n = 0, 1, \cdots, N)$. u_j^n presents the approximation of $u(x_j, t_n)$. We define the finite difference operators as

$$f_j^{n+1/2} = \frac{f_j^{n+1} + f_j^n}{2}, \quad \delta_t^+ f_j^n = \frac{f_j^{n+1} - f_j^n}{\Delta t}.$$

The Crank-Nicolson finite difference method is adopted on the reduced problem in the interior domain:

$$\delta_t^+ u_j^n + \delta_x^3 u_j^{n+1/2} = h_j^{n+1/2},$$

with

$$\begin{aligned}
\delta_x^3 u_1^n &= -\frac{u_4^n - 6u_3^n + 12u_2^n - 10u_1^n + 3u_0^n}{2\Delta x^3}, \\
\delta_x^3 u_j^n &= \frac{u_{j+2}^n - 2u_{j+1}^n + 2u_{j-1}^n - u_{j-2}^n}{2\Delta x^3}, j = 2, 3, \cdots, J-2.
\end{aligned}$$

Now we focus on the discretization on the artificial boundaries. The discrete form of the local absorbing boundary conditions on Ω_b is given by

$$\begin{aligned}
u_J^{n+1/2} - g_r^{n+1/2} &= 0, \\
\delta_x^+ u_J^{n+1/2} + f_r^{n+1/2} &= 0, \\
g_r^{n+1/2} - \sum_{i=1}^{p} B_i w_i^{n+1/2} &= \delta_x^2 u_J^{n+1/2}, \\
f_r^{n+1/2} - \sum_{i=1}^{p} b_i v_i^{n+1/2} &= \delta_x^2 u_J^{n+1/2}, \\
(1 - a_i) v_i^{n+1/2} + a_i \delta_t^+ v_i^n &= f_r^{n+1/2} - \delta_t^+ f_r^n, \\
(1 - A_i) w_i^{n+1/2} + A_i \delta_t^+ w_i^n &= g_r^{n+1/2} - \delta_t^+ g_r^n,
\end{aligned}$$

where

$$\begin{aligned}
\delta_x^+ u_J^n &= \frac{u_{J-2}^n - 4u_{J-1}^n + 3u_J^n}{2\Delta x}, \\
\delta_x^2 u_J^n &= \frac{2u_J^n - 5u_{J-1}^n + 4u_{J-2}^n - u_{J-3}^n}{\Delta x^2}, \\
i &= 1, 2, \cdots, p.
\end{aligned}$$

Equally, the discretizations can be achieved for the local absorbing boundary

conditions on Ω_a as following:

$$\begin{aligned}
u_0^{n+1/2} - f_l^{n+1/2} + g_l^{n+1/2} &= 0, \\
f_l^{n+1/2} - \sum_{i=1}^{p} b_i \overline{v}_i^{n+1/2} &= \delta_x^+ u_0^{n+1/2}, \\
g_l^{n+1/2} - \sum_{i=1}^{p} B_i \overline{w}_i^{n+1/2} &= \delta_x^2 u_0^{n+1/2}, \\
(1-a_i)\overline{v}_i^{n+1/2} + a_i \delta_t^+ \overline{v}_i^n &= f_l^{n+1/2} - \delta_t^+ f_l^n, \\
(1-A_i)\overline{w}_i^{n+1/2} + A_i \delta_t^+ \overline{w}_i^n &= g_l^{n+1/2} - \delta_t^+ g_l^n,
\end{aligned}$$

where

$$\begin{aligned}
\delta_x^+ u_0^n &= -\frac{u_2^n - 4u_1^n + 3u_0^n}{2\Delta x}, \\
\delta_x^2 u_0^n &= \frac{2u_0^n - 5u_1^n + 4u_2^n - u_3^n}{\Delta x^2}, \\
i &= 1, 2, \cdots, p.
\end{aligned}$$

The finite difference scheme is second-order in both time and space.

2.5 Numerical results

In this section, we report the numerical results of linearized KdV equation with the local absorbing boundary conditions by Padé approximation to illustrate the effectiveness and stability of our proposed method.

Example 1. We consider the following problem [3]

$$\begin{aligned}
u_t + u_{xxx} &= 0, \qquad x \in \mathbb{R}, \\
u(x,0) &= e^{-x^2}, \ x \in \mathbb{R}, \\
u &\to 0, \qquad x \to \infty.
\end{aligned}$$

The fundamental solution of this linearized KdV equation is

$$u(x,t) = E(x,t) * e^{-x^2},$$

where $E(x,t) = \frac{1}{\sqrt[3]{3t}}\mathrm{Ai}(\frac{x}{\sqrt[3]{3t}})$, $\mathrm{Ai}(\cdot)$ is the Airy function, and $*$ denotes the convolution operator on the whole real axis. Since the Gaussian functions decay very fast, the initial condition can be taken to have a compact support. In this example, we choose the computational domain as $x \in [-6, 6]$.

In order to illustrate the performance of the proposed local ABCs, L_2 error and L_∞ error are tested, which are defined by

$$L_2(t) = \sqrt{\frac{1}{J+1}\sum_{j=0}^{J} |u_{ex}(x_j,t) - u_{nu}(x_j,t)|^2},$$

and

$$L_\infty(t) = \max_{j=0,1,\cdots,J}\{|u_{ex}(x_j,t) - u_{nu}(x_j,t)|\},$$

where u_{ex} and u_{nu} denote the exact solution and numerical solution of u, respectively.

Table 2.2: L_2 error and convergence order for the time space at $T = 2$.

	$\Delta t = \frac{1}{16}$	order	$\Delta t = \frac{1}{32}$	order	$\Delta t = \frac{1}{64}$	order
$p = 5$	1.870e-2	-	4.118e-3	2.18	8.797e-4	2.23
$p = 7$	1.884e-2	-	4.680e-3	2.01	1.227e-3	1.93
$p = 9$	1.866e-2	-	4.587e-3	2.02	1.135e-3	2.01

For temporal error analysis, we choose $\Delta x = \frac{1}{2^{11}}$ such that the error in spatial discretization can be ignored. Table 2.2 lists the L_2 error and convergence order for time space with different values of parameter p. This table demonstrates that the convergence order is almost to 2 for time space.

For spatial error analysis, we choose time step $\Delta t = 10^{-3}$, such that the temporal error can be neglected. The errors and convergence order for spatial space with different p at time $T = 2$ and $T = 4$ are presented in Tables 2.3-2.4, respectively. We can conclude that the second-order convergency of the spatial error is clear when $p \geq 5$. Moreover, Fig. 2.4 plots the numerical solution and exact solution at different

Table 2.3: L_2 error and convergence order for the spatial space at $T = 2$.

	$\Delta x = \frac{1}{16}$	order	$\Delta x = \frac{1}{32}$	order	$\Delta x = \frac{1}{64}$	order
$p = 3$	4.101e-3	-	1.770e-3	1.21	1.207e-3	0.55
$p = 5$	3.044e-3	-	7.048e-4	2.11	1.283e-4	2.46
$p = 7$	3.120e-3	-	7.796e-4	2.00	2.007e-4	1.96
$p = 8$	3.107e-3	-	7.669e-4	2.02	1.881e-4	2.03
$p = 9$	3.110e-3	-	7.694e-4	2.02	1.906e-4	2.01

Table 2.4: L_2 error and convergence order for the spatial space at $T = 4$.

	$\Delta x = \frac{1}{16}$	order	$\Delta x = \frac{1}{32}$	order	$\Delta x = \frac{1}{64}$	order
$p = 3$	2.067e-3	-	9.024e-4	1.20	6.216e-4	0.54
$p = 5$	1.542e-3	-	3.649e-4	2.08	7.221e-5	2.34
$p = 7$	1.568e-3	-	3.904e-4	2.01	9.720e-5	2.01
$p = 8$	1.567e-3	-	3.900e-4	2.01	9.682e-5	2.01
$p = 9$	1.568e-3	-	3.907e-4	2.00	9.758e-5	2.00

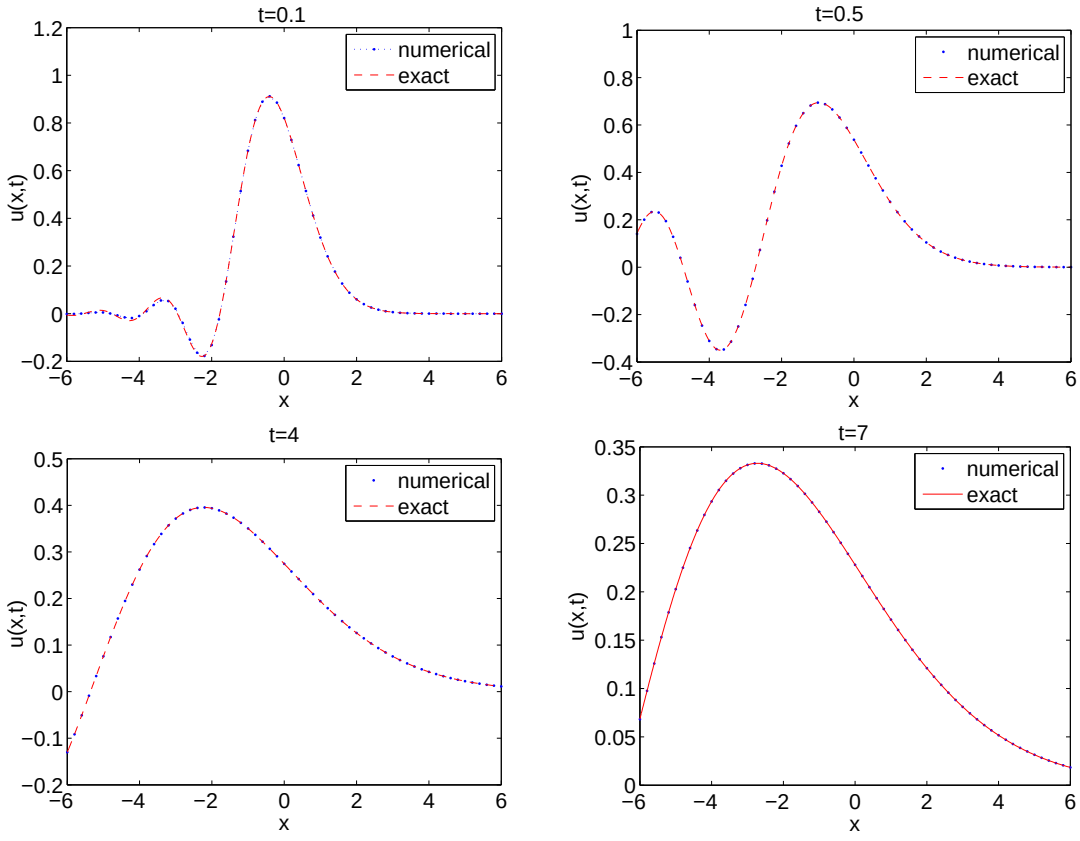

Figure 2.4: Numerical solutions compared with exact solutions at different times as the parameter $p = 7$.

times with the mesh sizes $\Delta t = 0.02$ and $\Delta x = 0.02$ as the parameter $p = 7$. This figure shows that the numerical solution matches the exact solution very well. This figure also illustrates that the reflection waves are negligible at the artificial boundaries, when the waves travel out of the computational domain.

Table 2.5: L_2 error and convergence order for the time space at $T = 7$.

	$\Delta t = \frac{1}{16}$	order	$\Delta t = \frac{1}{32}$	order	$\Delta t = \frac{1}{64}$	order
$p = 6$	5.922e-4	-	1.374e-4	2.11	2.770e-5	2.31
$p = 7$	6.061e-4	-	1.503e-4	2.01	3.711e-5	2.02
$p = 9$	6.065e-4	-	1.505e-4	2.01	3.732e-5	2.01

In order to test the stability of the overall finite difference scheme for long time, we list the L_2 error and convergence order for the time space at $T = 7$ in Table 2.5. From this table, one can see that the convergence order for the time space is almost to 2, and the finite difference scheme is unconditionally stable for long time calculations.

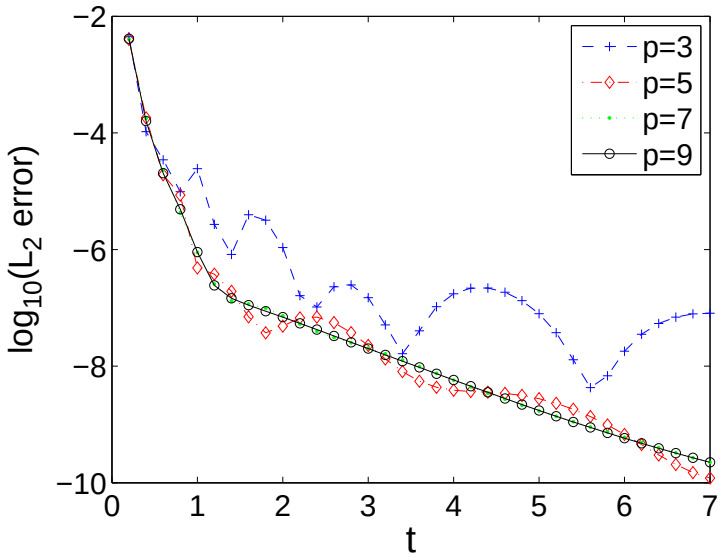

Figure 2.5: Numerical errors in L_2 norm with different p for time $T = 7$.

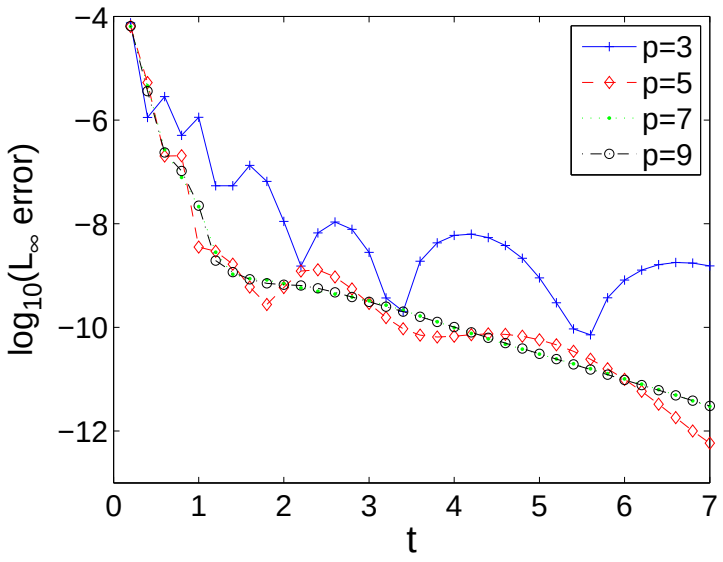

Figure 2.6: Numerical errors in L_∞ norm with different p for time $T = 7$.

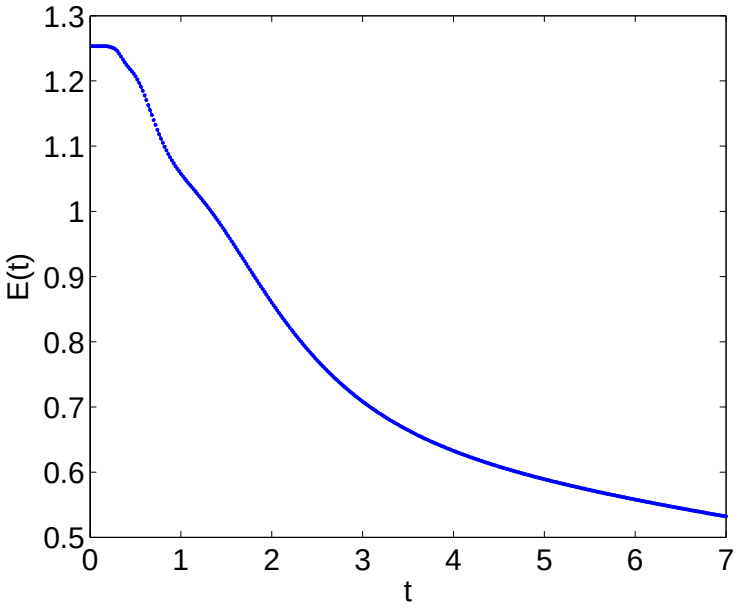

Figure 2.7: The energy of the wave remaining in the bounded domain.

Figs. 2.5-2.6 depict the L_2 and L_∞ error with different parameter p for time $T = 7$. Both L_2 and L_∞ error decay over time, since the wave is propagating away from the area we are monitoring. We define the energy of the linearized KdV equation on the bounded domain by the expression $E(t) = \int_a^b u^2(x,t)dx$, which can be calculated numerically through the numerical quadrature. In Fig. 2.7, we plot the energy of the wave remaining in the bounded domain with the mesh sizes $\Delta t = 0.02$ and $\Delta x = 0.02$. As the wave moves away from the bounded domain, the energy decays accordingly. From the figures, one can observe that long time calculations with local ABCs are stable.

Example 2. We choose the initial condition as

$$u(x,0) = \sin(5x)e^{-x^2/4}.$$

The computational domain is $x \in [-6, 6]$.

The numerical solutions and exact solutions at different times are presented in Fig. 2.8. From this figure, we can observe that the numerical solutions show an agreement with the exact solutions, and there is no dramatic reflection when the wave travels through the left artificial boundary.

Fig. 2.9 plots the energy of the wave in the finite computational domain. We can see that the energy gradually decreases to zero, while the wave moves out of the computational domain. This figure implies that the local absorbing boundary conditions are nearly transparent for the wave propagation.

2.6 Concluding remarks

In our work, highly accurate local absorbing boundary conditions for a linearized KdV equation is proposed. Applying the absorbing boundary conditions yields an equivalent initial boundary value problem defined on a finite domain. The stability of the reduced initial boundary value problem is analyzed. In order to test the efficiency and stability of the reduced initial boundary value problem, a second-

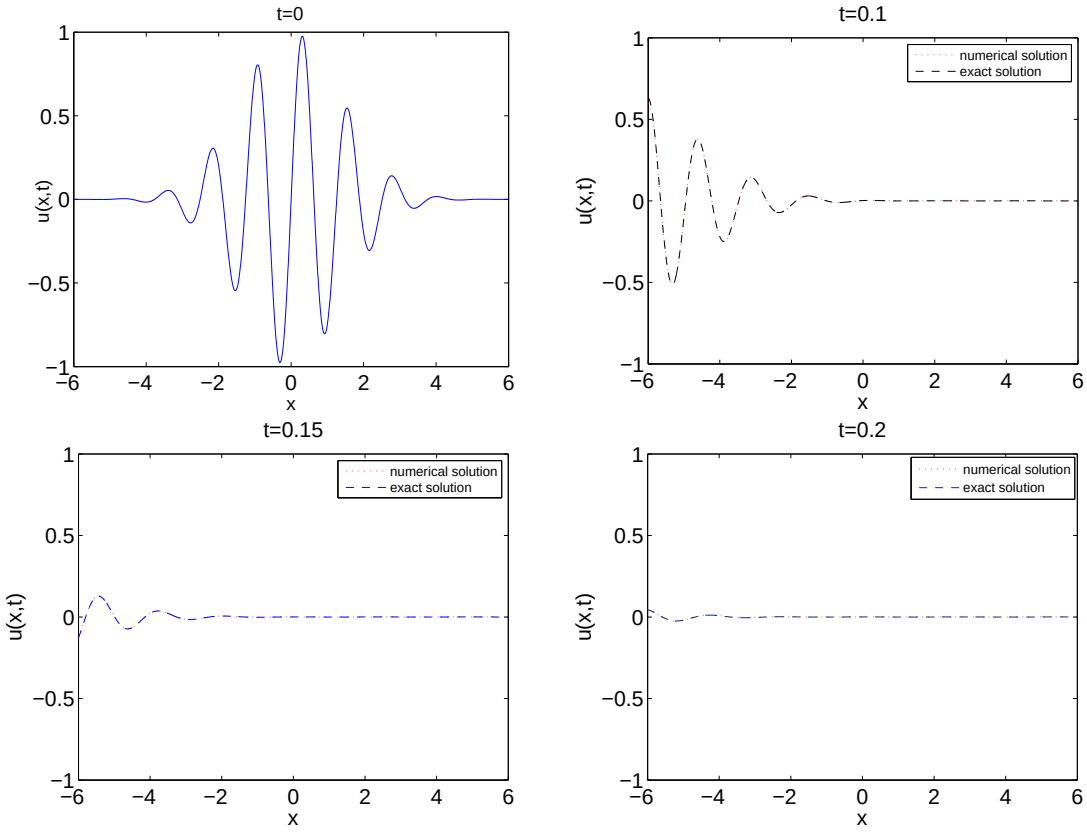

Figure 2.8: Numerical solutions compared with exact solutions at different times as the parameter $p = 9$.

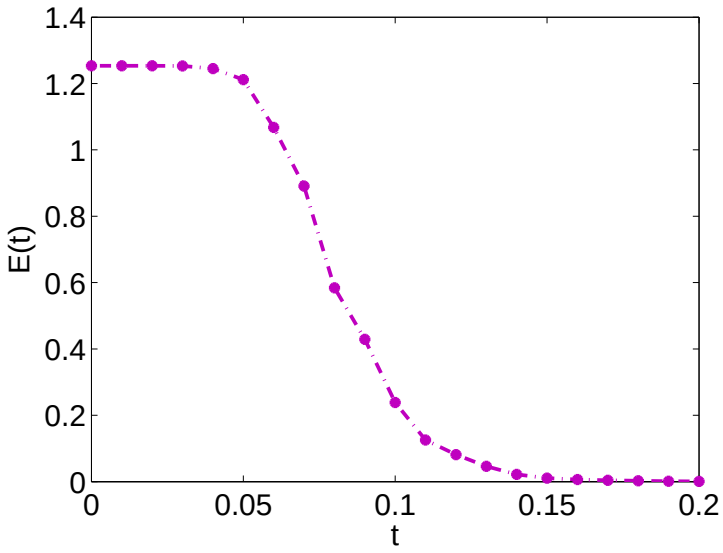

Figure 2.9: The energy of the wave remaining in the bounded computational domain.

order finite difference method is established and applied. The numerical results are presented to demonstrate the stability and accuracy of the proposed method. Future research directions will include yielding different approximations of $\sqrt[3]{s}$ to improve the accuracy and efficiency of the local ABCs. The second direction of research would be to design the local ABCs for the fully nonlinear and multi-dimensional KdV equation on unbounded domain.

Chapter 3

Continued fraction local absorbing boundary conditions for linearized KdV equation

3.1 Introduction

The main difficulty of calculating wave propagations on unbounded domains is the efficiency and accuracy. The most popular way to tackle this kind of problems is to establish suitable absorbing boundary conditions, which can truncate the domain of interest into a bounded region. The original unbounded PDE will become a initial-value problem on a bounded region. We are able to solve for numerical solutions properly. The crucial point is to construct suitable ABC's that simulate the omitted exterior effectively and accurately.

Due to the large computation cost for global ABC's, we prefer to construct local absorbing boundary conditions. Comparing to global ABC's, local ABC's are time-saving with less computation cost. Local ABC's are computationally inexpensive and effectively annihilate the reflecting waves from the artificial boundaries, despite the little sacrifice on the accuracy. Engquist and Majda [7] proposed the perfectly local absorbing boundary conditions for general classes of linear wave equations. However, it is limited by the difficulties posed in applying the high-order derivatives in the practical computations. High-order derivatives will cause inconvenience while implementing finite element methods or finite difference methods. The main prob-

lem is that we cannot use $\mathbb{C}^{\nu}$ finite elements to estimate high order derivatives effectively. Safjan [14] developed a family of highly accurate local non-reflecting boundary operators to solve unbounded wave-type equations. He introduced the multi-stage boundary operators, which can achieve arbitrary accuracy without acquiring extra information of high-order derivatives beforehand. Guddati and Tassoulas [15] also surmounted the difficulty and proposed a continued fraction method to obtain the absorbing boundary conditions that contain only second-order derivatives. In this way, they added auxiliary variables next to the boundary, so as to get extra degrees of freedom while encountering higher order local boundary conditions. Moreover, the resulting coefficient matrix has very good properties, such as symmetric and positive-definite. The advantage of Guddati and Tassoulas's method are easy to implement numerically and easy to increase to arbitrary order. Zheng *et al.* [3] constructed the global (exact) absorbing boundary conditions for a linearized KdV equation and developed a fast evaluation method to reduce the computational cost of convolution operations involved in the global ABCs. A kind of non-reflecting boundary conditions which are suitable for numerical purposes are presented in [5], and the discretization of the non-reflecting boundary conditions is studied in detail. While the local ABCs are local in both space and time, which are computationally efficient and tractable. This chapter is devoted to studying the numerical solution of a linearized KdV equation on unbounded domain with continued fraction local ABC's. Based on Zheng *et al.* [3]'s method, we can obtain the artificial boundary conditions in frequency domain. Inspired by Guddati and Tassoulas [15], we provide a way in the approximation of $\sqrt[3]{s}$ with continued fraction. Three local boundary conditions can therefore be derived. It is convenient to improve the accuracy by increasing the number of fraction layers. Some numerical examples are tested in the last section.

3.2 Governing equation

The initial value problem of a linearized KdV equation is given by the following form

$$\begin{aligned} u_t + u_{xxx} &= h(x,t),\ x \in \mathbb{R}, t \in [0,T], && (3.1)\\ u(x,0) &= u_0(x),\ \ x \in \mathbb{R}, && (3.2)\\ u &\to 0, \qquad |x| \to +\infty, && (3.3) \end{aligned}$$

where $h(x,t)$ and $u_0(x)$ denote source term and initial condition with compactly supports, i.e., there is a finite interval $[a,b]$ such that $\text{Supp}\{h(x,t) \subset [a,b] \times [0,T]\}$, and $\text{Supp}\{u_0(x) \subset [a,b]\}$.

We introduce the following artificial boundaries as in [3]:

$$\begin{aligned} \Omega_a &= \{(x,t)|x = a,\ 0 \le t \le T\},\\ \Omega_b &= \{(x,t)|x = b,\ 0 \le t \le T\}. \end{aligned}$$

The unbounded domain $\mathbb{R}^1 \times [0,T]$ are divided into three parts by the artificial boundaries Ω_a and Ω_b, namely, the bounded domain $D_i = [a,b] \times [0,T]$, and the unbounded parts $D_L = (-\infty, a] \times [0,T]$ and $D_R = [b, +\infty) \times [0,T]$. The numerical solution of linearized KdV equation on unbounded domain can be obtain by finding the boundary conditions on the artificial boundaries Ω_a and Ω_b and reducing the original problem into an initial boundary value problem on the finite computational domain.

Next, we consider the three problems on D_i, D_L and D_R respectively:

$$\begin{aligned} u_t + u_{xxx} &= 0, \qquad x > b, 0 \le t \le T, && (3.4)\\ u(x,t)|_{x=b} &= u(b,t),\ 0 \le t \le T, && (3.5)\\ u(x,0) &= 0, \qquad x > b, && (3.6)\\ u &\to 0, \qquad x \to +\infty, && (3.7) \end{aligned}$$

and

$$\begin{aligned} u_t + u_{xxx} &= 0, \qquad x \in [a,b], 0 \le t \le T, && (3.8)\\ u(x,t)|_{x=a} &= u(a,t),\ 0 \le t \le T, && (3.9)\\ u(x,t)|_{x=b} &= u(b,t),\ 0 \le t \le T, && (3.10)\\ u(x,0) &= u_0(x,0),\ 0 \le t \le T, && (3.11)\\ & && (3.12) \end{aligned}$$

and

$$\begin{aligned} u_t + u_{xxx} &= 0, \qquad x < a, 0 \le t \le T, && (3.13)\\ u(x,t)|_{x=a} &= u(a,t),\ 0 \le t \le T, && (3.14)\\ u(x,0) &= 0, \qquad x < a, && (3.15)\\ u &\to 0, \qquad x \to -\infty. && (3.16) \end{aligned}$$

The problems, (3.4)-(3.7) and (3.13)-(3.16), can be solved if the boundary conditions are given. Applying the Laplace transformation to equations (3.4)-(3.7), we obtain

$$s\hat{u} + \hat{u}_{xxx} = 0, \tag{3.17}$$

The general solution of equation (3.17) can be found as

$$\hat{u}(x,s) = c_1(s)e^{\lambda_1(s)x} + c_2(s)e^{\lambda_2(s)x} + c_3(s)e^{\lambda_3(s)x}, \tag{3.18}$$

where

$$\lambda_1(s) = -\sqrt[3]{s}, \lambda_2(s) = -\sqrt[3]{s}\omega, \lambda_3(s) = -\sqrt[3]{s}\omega^2, \omega = e^{\frac{2\pi i}{3}}.$$

Thus, the boundary conditions in the frequency domain are given as

$$\begin{aligned} \hat{u}(b,s) - \frac{1}{\lambda_1^2(s)}\hat{u}_{xx}(b,s) &= 0, && (3.19)\\ \hat{u}_x(b,s) - \frac{1}{\lambda_1(s)}\hat{u}_{xx}(b,s) &= 0, && (3.20)\\ \hat{u}(a,s) + \frac{1}{\lambda_1(s)}\hat{u}_x(a,s) + \frac{1}{\lambda_1^2(s)}\hat{u}_{xx}(a,s) &= 0. && (3.21) \end{aligned}$$

The global absorbing boundary conditions can be derived by directly applying inverse Laplace transform on equations (3.19)-(3.21). It is natural to try to construct effective and accurate local absorbing boundary conditions instead of the exact ABCs and to avoid the expensive convolution operations in the inverse Laplace transformation. Inspired by Guddati and Tassoulas[15], we provide a continued fraction approximation of $\sqrt[3]{s}$ in the next section and obtain three local ABCs.

3.3 The continued fraction approximation

Consider $\lambda_1(s) = -\sqrt[3]{s}$, if $z = s - 1$, $f_0(z) = (1+z)^a$, define

$$\begin{aligned} f_0(z) &= f_0(0) + \frac{z}{f_1(z)} \\ f_{i-1}(z) &= f_{i-1}(0) + \frac{z}{f_i(z)}, \quad i = 1, 2, ... \end{aligned}$$

Thus, from last equation we can rewrite $f_i(z)$ in the form of $f_{i-1}(z)$'s and when z tends to 0, we have

$$f_i(0) = \lim_{x \to 0} \frac{x}{f_{i-1}(x) - f_{i-1}(0)} = \frac{1}{f'_{i-1}(0)}$$

namely,

$$f_0(0) = 1, f_1(0) = \frac{1}{f'_0(0)}, f_2(0) = \frac{1}{f'_1(0)}, \cdots, f_i(0) = \frac{1}{f'_{i-1}(0)}.$$

For simplicity, let's denote

$$P_i(z) = \frac{f_{i-1}(z) - f_{i-1}(0)}{z} = \frac{1}{f_i(z)}.$$

A system of equation can be obtained by taking n-th derivative on both side of $f_i(z)P_i(z) = 1$, i.e.

$$\begin{aligned} f_i(z)P_i(z) &= 1 \\ f'_i(z)P_i(z) + f_i(z)P'_i(z) &= 0 \\ &\cdots \\ f_i^{(n)}(z)P_i(z) + \cdots + f_i(z)P_i^{(n)}(z) &= 0, \text{ as } z \to 0. \end{aligned}$$

Since by Taylor expansion at 0,

$$P_i(z) = f'_{i-1}(0) + \frac{z}{2} f''_{i-1}(0) + \cdots$$

Therefore, as long as $f_{i-1}^{(n+1)}(0)$ is provided, $f_i^{(n)}(0)$ can be obtained inductively from above system of equations. It means if $f_m(0)$ is wanted, at least we need the information from $f_0(0)$ to m-th derivative of $f_0(0)$.

Moreover, the general formula for $f_i^{(n)}(0)$ is derived as

$$f_i^{(n)}(0) = -\frac{1}{P_i(0)}[\sum_{k=1}^{n} C_n^k f_i^{(n-k)}(0) P_i^{(k)}(0)],$$

with

$$P_i^k(0) = \frac{1}{k+1} f_{i-1}^{(k+1)}(0).$$

For simplicity, we denote $f_i(0) = f_i, \quad i = 1, 2, \ldots$, and

$$f_0(z) = 1 + \cfrac{s-1}{f_1 + \cfrac{s-1}{f_2 + \cfrac{s-1}{\cdots}}} \tag{3.22}$$

i.e. $\lambda_1(s) = -\sqrt[3]{s} = -(1 + B_1)$, with $B_i = \cfrac{s-1}{f_i + B_{i+1}}, i = 1, 2, \ldots$

Hence we can obtain λ_1^2, i.e. $s^{\frac{2}{3}}$ in the same way. λ_1^2 can be represented as,

$$\lambda_1^2(s) \;=\; 1 + \cfrac{s-1}{g_1 + \cfrac{s-1}{g_2 + \cfrac{s-1}{\cdots}}} \tag{3.23}$$

Likewise, we have $\lambda_1^2(s) = \sqrt[3]{s^2} = 1 + C_1$ with $C_i = \cfrac{s-1}{g_i + C_{i+1}}, i = 1, 2, \ldots.$

Fig. 3.1 show the approximation to $\sqrt[3]{s}$ with continued fraction method when $p = 8$ and $p = 16$. The corresponding error plots are also provided next to them. One can see that the continued fraction approximation performs better when p is larger.

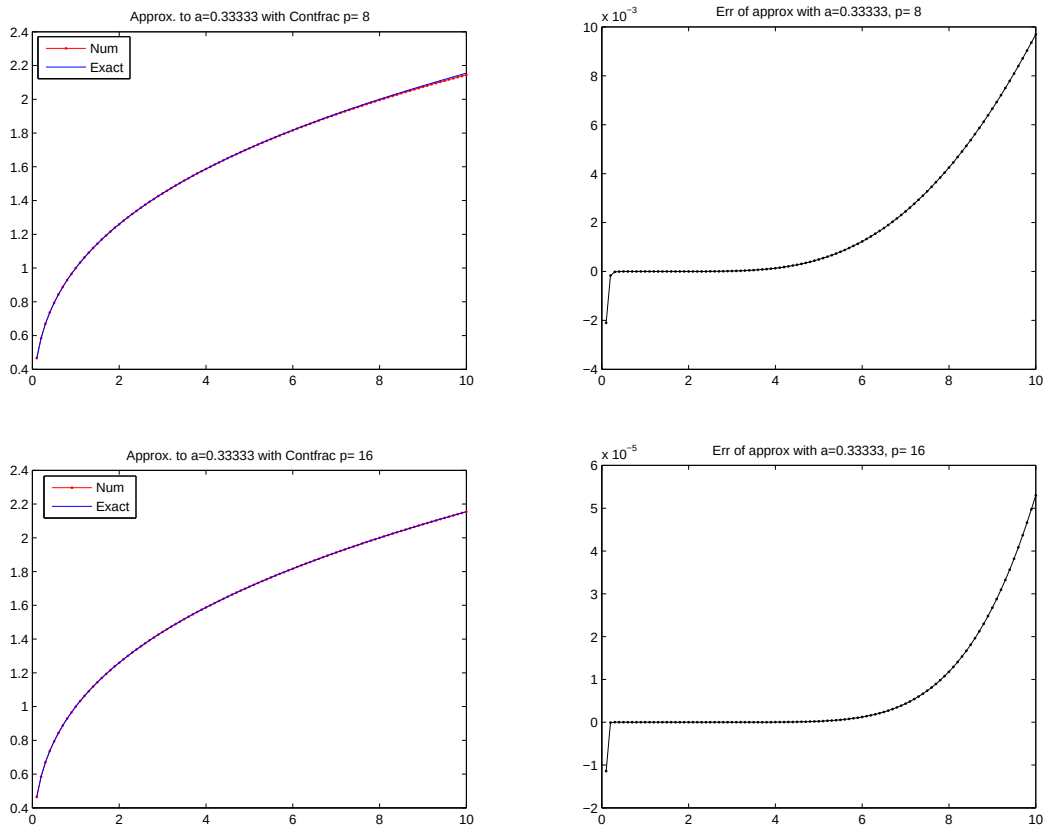

Figure 3.1: Continued fraction approximations of $\sqrt[3]{s}$ and corresponding error at different $p = 8, 16$.

3.4 The local absorbing boundary conditions

Right Boundary Conditions: $x > b$

1. $\hat{u}_x - \lambda_1 \hat{u} = 0$, where $\lambda_1 = -\sqrt[3]{s}$

   Let's define a group of auxiliary variables as

   $$\hat{w}_1 = B_1 \hat{u}, \hat{w}_i = B_i \hat{w}_{i-1}, i = 2, 3, \ldots, p-1, B_p = \frac{s-1}{f_p},$$

   then the first right boundary condition in the frequency domain is approximated as follows:

   $$\begin{aligned} \hat{u}_x + \hat{u} + \hat{w}_1 &= 0 \\ f_1 \hat{w}_1 + \hat{w}_2 &= (s-1)\hat{u} \\ f_i \hat{w}_i + \hat{w}_{i+1} &= (s-1)\hat{w}_{i-1}, i = 2, \ldots, p-1 \\ f_p \hat{w}_p &= (s-1)\hat{w}_{p-1} \end{aligned}$$

   After performing inverse Laplace transform on the above system (with f_i's are constants), we will obtain a system of equations

   $$\begin{aligned} u_x + u + w_1 &= 0 && (3.24) \\ f_1 w_1 + w_2 &= \frac{d}{dt}u - u && (3.25) \\ f_i w_i + w_{i+1} &= \frac{d}{dt}w_{i-1} - w_{i-1}, i = 2, \ldots, p-1 && (3.26) \\ f_p w_p &= \frac{d}{dt}w_{p-1} - w_{p-1} && (3.27) \end{aligned}$$

2. $\hat{u}_{xx} - \lambda_1^2 \hat{u} = 0$, where $\lambda_1 = -\sqrt[3]{s}$

   Define another group of auxiliary variables as

   $$\hat{v}_1 = C_1 \hat{u}, \hat{v}_i = C_i \hat{v}_{i-1}, \quad i = 2, 3, \ldots, p-1 \ , \ C_p = \frac{s-1}{g_p}.$$

Then the second right boundary condition in the frequency domain is approximated as:

$$\begin{aligned}
\hat{u}_{xx} - \hat{u} - \hat{v}_1 &= 0 \\
g_1\hat{v}_1 + \hat{v}_2 &= (s-1)\hat{u} \\
g_i\hat{v}_i + \hat{v}_{i+1} &= (s-1)\hat{v}_{i-1}, i = 2, \ldots, p-1 \\
g_p\hat{v}_p &= (s-1)\hat{v}_{p-1}
\end{aligned}$$

After performing inverse Laplace transformation on above system,(g_i's are constants)

$$\begin{aligned}
u_{xx} - u - v_1 &= 0 && (3.28)\\
g_1v_1 + v_2 &= \frac{d}{dt}u - u && (3.29)\\
g_iv_i + v_{i+1} &= \frac{d}{dt}v_{i-1} - v_{i-1}, i = 2, \ldots, p-1 && (3.30)\\
g_pv_p &= \frac{d}{dt}v_{p-1} - v_{p-1} && (3.31)
\end{aligned}$$

Left Boundary Conditions: $x < a$

1. $\hat{u}_{xx} + \lambda_1\hat{u}_x + \lambda_1^2\hat{u} = 0$, where $\lambda_1 = -\sqrt[3]{s}$

$$\text{Define} \begin{cases} \hat{\bar{w}}_1 = C_1\hat{u} \quad \hat{\bar{w}}_i = C_i\hat{\bar{w}}_{i-1} = \dfrac{s-1}{g_i + C_{i+1}}\hat{\bar{w}}_{i-1}; \\ \qquad\qquad\qquad\qquad\qquad\qquad\qquad\qquad , i = 2, \ldots, p-1, \\ \hat{\bar{v}}_1 = B_1\hat{u}_x \quad \hat{\bar{v}}_i = B_i\hat{\bar{v}}_{i-1} = \dfrac{s-1}{f_i + B_{i+1}}\hat{\bar{v}}_{i-1}. \end{cases}$$

where C_i, B_i are defined as in section 3.3.

With continued fraction approximation to λ_1^2, we take inverse Laplace transform

on the group of ABC's on the left boundary and get

$$u_{xx} - u_x + u - \bar{v}_1 + \bar{w}_1 = 0 \tag{3.32}$$

$$f_1\bar{v}_1 + \bar{v}_2 = \frac{d}{dt}u_x - u_x \quad ; \quad g_1\bar{w}_1 + \bar{w}_2 = \frac{d}{dt}u - u \tag{3.33}$$

$$f_i\bar{v}_i + \bar{v}_{i+1} = \frac{d}{dt}\bar{v}_{i-1} - \bar{v}_{i-1} \quad ; \quad g_i\bar{w}_i + \bar{w}_{i+1} = \frac{d}{dt}\bar{w}_{i-1} - \bar{w}_{i-1} \tag{3.34}$$

$$f_p\bar{v}_p = \frac{d}{dt}\bar{v}_{p-1} - \bar{v}_{p-1} \quad ; \quad g_p\bar{w}_p = \frac{d}{dt}\bar{w}_{p-1} - \bar{w}_{p-1} \tag{3.35}$$

Coupling equations (3.24)-(3.27), (3.28)-(3.31) and (3.32)-(3.35), we therefore attain the local boundary conditions based on continued fraction method for the linearized KdV equation. Combine with subproblem(3.8)-(3.11). One has an initial boundary value problem.

3.5 Numerical results

In this section, we report the numerical results of linearized KdV equation with continued fraction based local absorbing boundary conditions to illustrate the effectiveness and accuracy of our proposed method.

Example 1. Let's re-visit the example 1 in Chapter 2. Consider the following problem [3]

$$\begin{aligned} u_t + u_{xxx} &= 0, \qquad x \in \mathbb{R}, \\ u(x,0) &= e^{-x^2}, \ x \in \mathbb{R}, \\ u &\to 0, \qquad x \to \infty. \end{aligned}$$

The fundamental solution of this linearized KdV equation is

$$u(x,t) = E(x,t) * e^{-x^2},$$

where $E(x,t) = \frac{1}{\sqrt[3]{3t}}\mathrm{Ai}(\frac{x}{\sqrt[3]{3t}})$, $\mathrm{Ai}(\cdot)$ is the Airy function, and $*$ denotes the convolution operator on the whole real axis. In this example, we choose the computational domain as $x \in [-6, 6]$.

In order to illustrate the performance of the proposed local ABCs, L_2 error and L_∞ error are tested, which are defined by

$$L_2(t) = \left(\frac{1}{J+1} \sum_{j=0}^{J} |u_{ex}(x_j, t) - u_{nu}(x_j, t)|^2 \right)^{\frac{1}{2}},$$

and

$$L_\infty(t) = \max_{j=0,1,\cdots,J} \{|u_{ex}(x_j, t) - u_{nu}(x_j, t)|\},$$

where u_{ex} and u_{nu} denote the exact solution and numerical solution of u, respectively.

Table 3.1: L_2 error and convergence order for the time space at $T = 1$.

	$\Delta t = \frac{1}{24}$	order	$\Delta t = \frac{1}{36}$	order	$\Delta t = \frac{1}{54}$	order	$\Delta t = \frac{1}{81}$	order
$p = 10$	2.600e-4	-	1.166e-4	1.98	4.929e-5	2.12	2.286e-5	1.89
$p = 12$	2.652e-4	-	1.194e-4	1.97	5.139e-5	2.08	2.325e-5	1.96

As we know, the numerical error mainly consists of the truncated error from the continued fraction, time and spatial discretization. Since the numerical error with the local ABCs adopting continued fraction method decays very fast to the level of the truncated error from the continued fraction, we pick larger p to see the convergence order in a clear view. For temporal error analysis, $\Delta x = \frac{1}{2^{11}}$ and therefore we can ignore the errors caused by the spatial discretization. Table 3.1 lists the L_2 error and convergence order for time space with different values of parameter $p = 10, 12$. This table indicates that the convergence order is almost to 2 for time space.

Table 3.2: L_2 error and convergence order for the spatial space at $T = 1$.

	$\Delta x = \frac{1}{5}$	order	$\Delta x = \frac{1}{10}$	order	$\Delta x = \frac{1}{20}$	order	$\Delta x = \frac{1}{40}$	order
$p = 9$	5.800e-3	-	1.300e-3	2.18	2.793e-4	2.20	4.859e-5	2.52
$p = 10$	6.000e-3	-	1.400e-3	2.15	3.422e-4	1.98	9.418e-5	1.86
$p = 12$	7.700e-3	-	1.500e-3	2.40	3.164e-4	2.20	7.474e-5	2.08

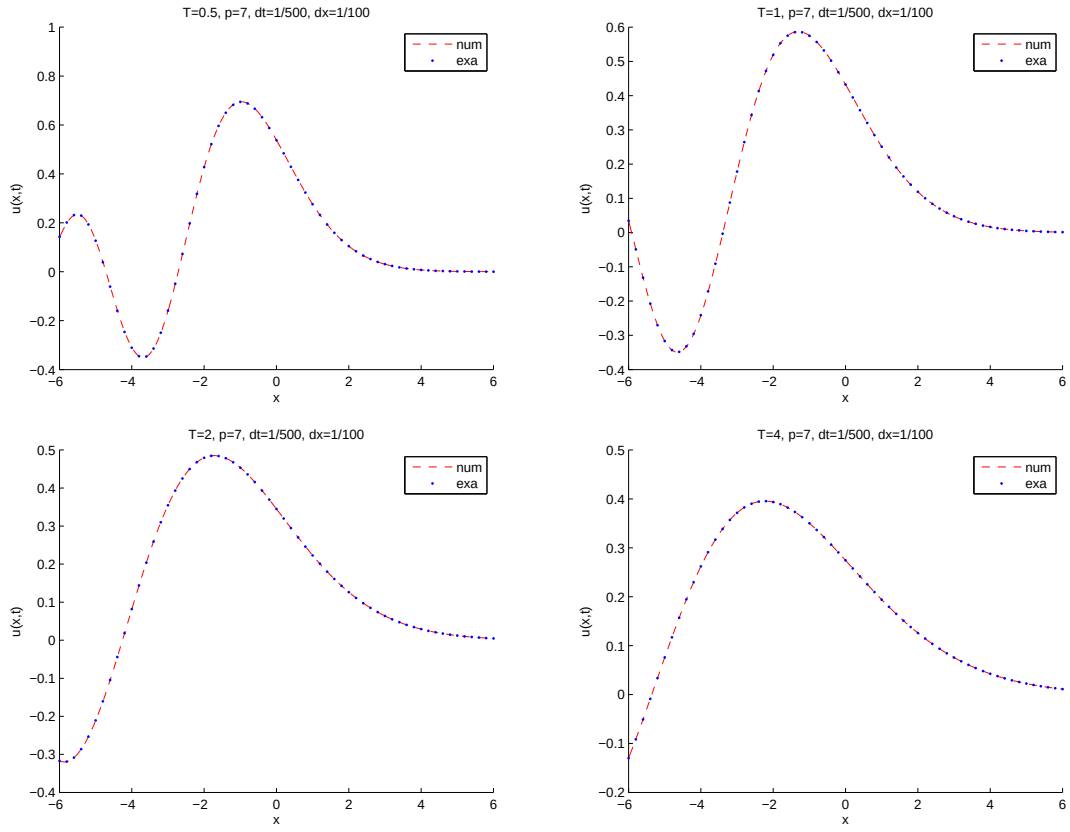

Figure 3.2: Numerical solutions compared with exact solutions at different times as the parameter $p = 7$.

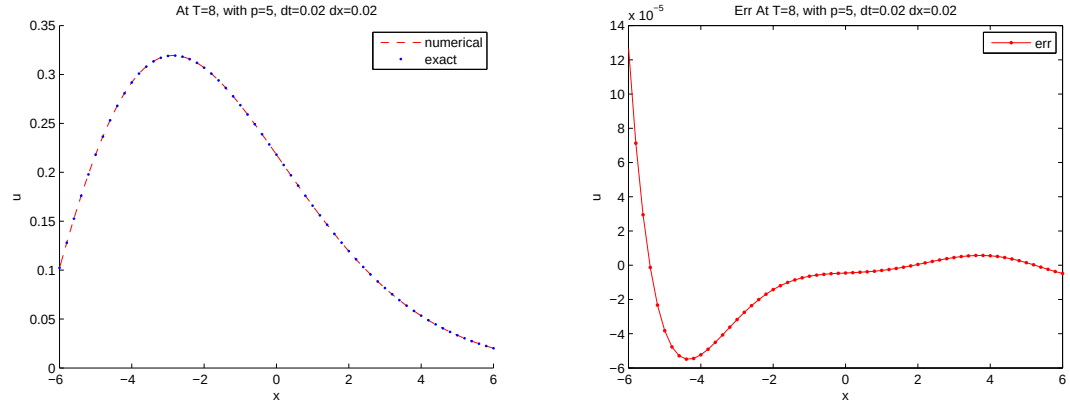

Figure 3.3: Numerical solutions compared with exact solutions at $T = 8$ with parameter $p = 5$.

For spatial error analysis, we choose time step $\Delta t = 2^{-10}$, such that the temporal error can be neglected. The errors and convergence order for spatial space with different p at time $T = 1$ are presented in Tables 3.2, respectively. As seen in $p = 10$ and $p = 12$, the convergence rate is nearly 2. In this example, we may conclude that the second order convergence of the spatial error is clear. Fig. 3.2 plots the numerical solution and exact solution at T=0.5s, 1s, 2s and 4s correspondingly with the mesh sizes $\Delta t = 1/500$ and $\Delta x = 1/100$ as the parameter $p = 7$. The numerical solution coincides the exact solution very well in Fig. 3.2. Moreover, in Fig.3.3 which plots the numerical solution and exact solution at $T = 8$ with $p = 5$. Even with small p and long computation time, the estimation performs still well with the error around 10^{-5}.

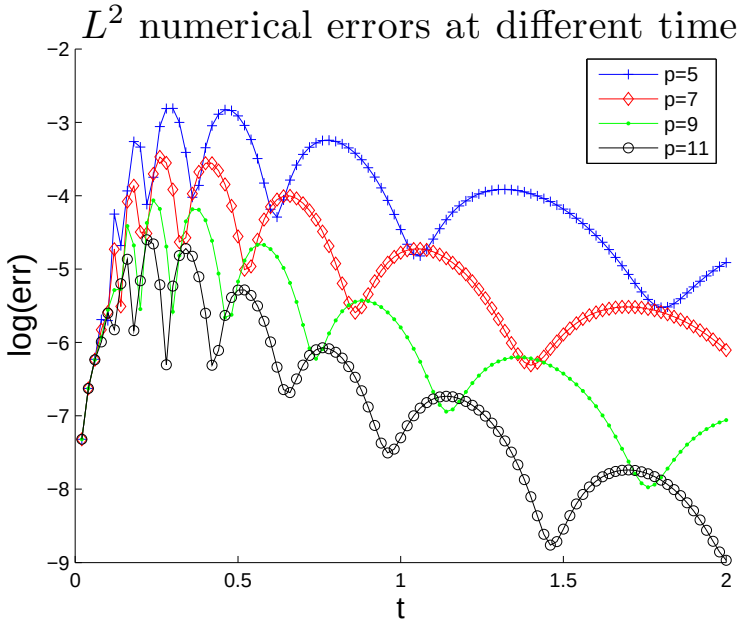

Figure 3.4: Numerical errors in L_2 norm with different p for time $T = 2$.

Figs. 3.4 - Fig. 3.5 summarize the L_2 and L_∞ error with different parameter p for time $T = 2$ as $dt = 1/500$ and $dx = 1/200$. Both L_2 and L_∞ error decay over time, since the wave is propagating outward. As defined in Chapter 2, the energy of the linearized KdV equation on the bounded domain adopts the expression

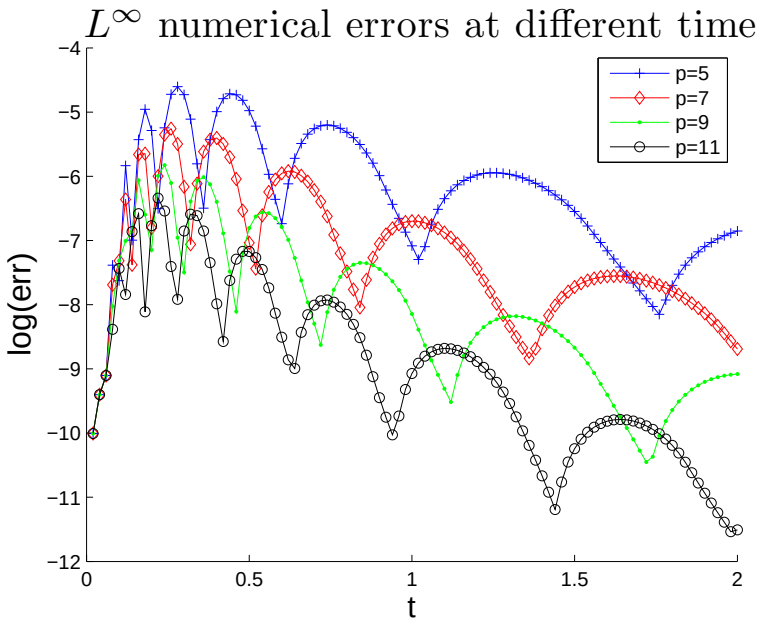

Figure 3.5: Numerical errors in L_∞ norm with different p for time $T = 2$.

$E(t) = \int_a^b u^2(x,t)dx$, which can be calculated numerically through the numerical quadrature. In Fig. 3.6, we plot the energy of the wave remaining in the bounded domain with the mesh sizes $\Delta t = 0.02$ and $\Delta x = 0.02$, $p = 5$ and $p = 10$ accordingly. For both p, as the wave moves away from the bounded domain, the energy decays accordingly. From the figures, one can observe that long time calculations with local ABCs are both stable with either small choice of p or large p.

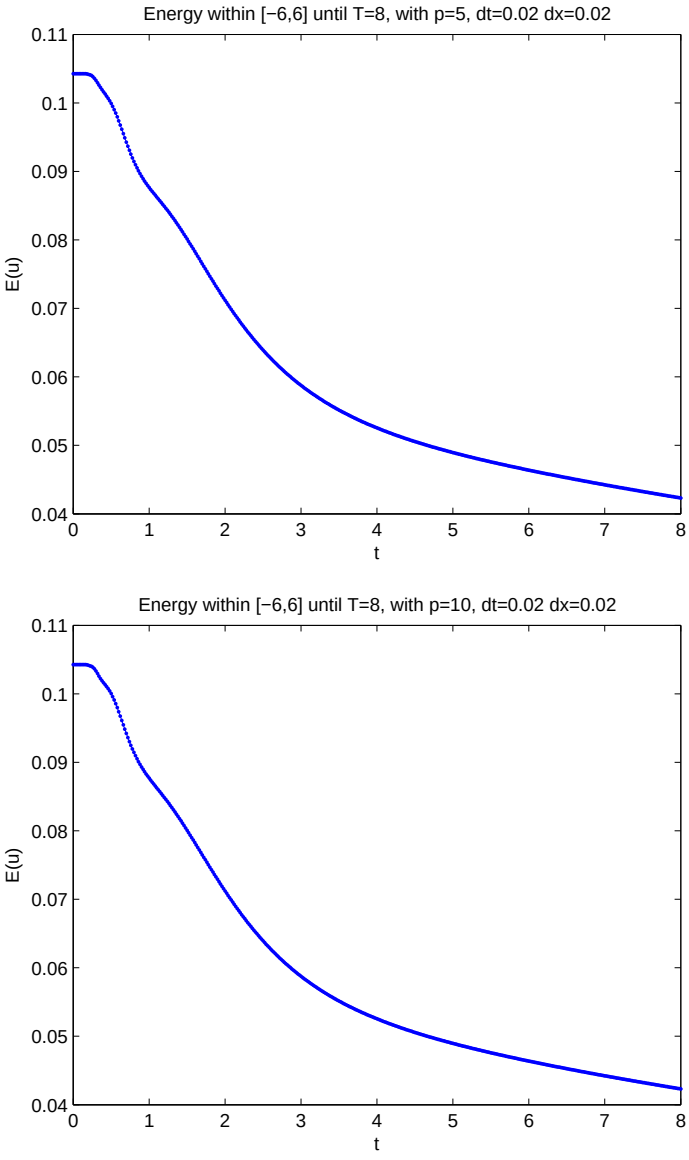

Figure 3.6: The energy of the wave remaining in the bounded domain $[-6, 6]$ with different parameter $p = 5$ and $p = 10$.

Chapter 4

Local absorbing boundary conditions for nonlinear KdV equations

4.1 Introduction

The governing equation of the Korteweg-de Vries equation usually adopts the form

$$u_t + u_{xxx} \pm 6uu_x = 0.$$

Many exact or analytical solutions of KdV equation with proper initial conditions are commonly obtained by the inverse scattering transform method [41, 44, 50], while the numerical solutions can be approximated by the finite element method [51] and the finite difference scheme such as the Zabusky-Kruskal scheme [40], Goda scheme [52] and more refer to Taha's work [45].

Despite some particular problems such as linearized equations [13, 3] or some special types of equations like the Burger's type equations [24, 25], it is still a tough job to give proper absorbing boundary conditions in general for nonlinear equations. Xu *et al.* [27, 28] developed the split local absorbing boundary conditions for 1-D and 2-D nonlinear Schrödinger equations.The local ABCs were acquired for the split linear subproblem and a full scheme was yielded then by coupling the discretizations of the interior equation and boundary subproblems. In 2008, a unifying approach is applied by Zhang *et al.* in [17, 18] to solve nonlinear Schrödinger equations. Later on

in [19, 20, 30], the method has been successfully applied to construct local ABCs for semi-linear parabolic equations and nonlinear wave equations on unbounded domain. The idea of the unifying approach to local absorbing boundary conditions comes from the operator splitting method and Strang splitting method which was first presented by Gilbert Strang in 1968 [55]. The key point is based on the operator split method. Recent years, Zheng [5] designed a kind of exact non-reflecting boundary conditions for modified KdV equation based on [46]. However, the extension of the exact NRBCs to the nonlinear KdV equation does not go out as straight forward as it was expected. Zheng, Wen and Han [3] derived exact ABCs to a linearized KdV problem. They also utilized the dual-Petrov-Galerkin spectral method, which was proposed by Shen [54] for numerical approximation. Moreover, the fast evaluation method was used in their work as a compensation to the computational cost caused by the global absorbing boundary conditions. The stability of the reduced problem was proved in [3].

In this chapter, based on the local absorbing boundary conditions we derived in the Chapter 2 and Chapter 3, we attempt to extend the local ABCs to the nonlinear KdV equation using the unifying approach to split absorbing boundary conditions. We construct the local absorbing boundary conditions for linear subproblem, and then using the unifying approach, an approximation of the local artificial boundary conditions for nonlinear KdV equations is given. A nonlinear problem on unbounded domain therefore becomes a reduced problem on a finite area. Numerical scheme is implemented to the reduced initial boundary value problem. Finally several numerical examples are given to demonstrate the effectiveness of our local ABCs.

4.2 Design of the local absorbing boundary conditions for KdV equation

In this section, we consider the nonlinear Korteweg-de Vries equation defined on unbounded domain

$$\begin{aligned} u_t + u_{xxx} + 6uu_x &= 0,\ x \in \mathbb{R}, t > 0, && (4.1)\\ u(x,0) &= u_0(x),\quad x \in \mathbb{R}, && (4.2)\\ u &\to 0, \qquad |x| \to +\infty, && (4.3) \end{aligned}$$

The initial function $u_0(x)$ is assumed to be compactly supported on the finite interval [a, b]. We aim at constructing the nonlinear local absorbing boundary conditions for Eq (4.1)-(4.3).

4.2.1 A review on the unifying approach to split ABCs

The unifying approach to split ABCs is applied by Zhang *et al.* in [17, 18]. The underlying idea is abstracting from the famous time-split method. Basically, the steps of achieving the unifying approach include

- Divide the original problem into linear and nonlinear subproblems and set up artificial boundaries.
- Distinguish the inward and outward waves along the artificial boundaries for the linear subproblem.
- Approximate the corresponding linear operator the "one-way operator" which ensures the wave going outward.
- Unite the approximated linear subproblem and the nonlinear subproblem to yield the nonlinear absorbing boundary conditions.

Taking our concerned problem as an example.

First of all, let's rewrite the governing equation (4.1) into

$$\frac{\partial u(x,t)}{\partial t} \equiv [\mathbf{L}+\mathbf{N}]u(x,t),\ x \in \mathbb{R}, t > 0, \tag{4.4}$$

where $\mathbf{L}$ stands for the linear differential operator and $\mathbf{N}$ represents the nonlinear differential operator. For the whole axis,

$$\mathbf{L}u := -\frac{\partial^3}{\partial x^3}[u] \quad \text{and} \quad \mathbf{N}u := -3\frac{\partial}{\partial x}[u^2]. \tag{4.5}$$

The time-splitting method suggests that from time t to $t+\tau$ for a small enough τ, the exact solution of Eq. 4.4 can be estimated as

$$u(x,t+\tau) \approx e^{\mathbf{L}\tau}e^{\mathbf{N}\tau}u(x,t). \tag{4.6}$$

In analog of famous Strang splitting method [55],

$$u(x,t+\tau) \approx e^{\mathbf{L}\tau/2}e^{\mathbf{N}\tau}e^{\mathbf{L}\tau/2}u(x,t). \tag{4.7}$$

Based on the result in Chapter 2 and Chapter 3, we manage to obtain the local ABCs for the linear subproblems. Our target is to obtain the local ABCs which can be easily applied to nonlinear problems. Therefore, it is reasonable to follow Eq. (4.6) with the time-splitting method since it captures the information from both linear and nonlinear energy with a simple form. The idea of unifying approach is to derive the approximated operator $\hat{\mathbf{L}}$ for the linear operator $\mathbf{L}$ by making the wave propagate away from the computational domain. Replace $\mathbf{L}$ in Eq. (4.6) and we arrive at the one-way equation by letting τ tends to zero and restricting to the artificial boundaries

$$u_t(x,t) = [\hat{\mathbf{L}}+\mathbf{N}]u(x,t). \tag{4.8}$$

As long as we have the approximation $\hat{\mathbf{L}}$, Eq. (4.8) will act as the local ABCs for nonlinear problem.

Recall the major steps in constructing the local ABCs for the linearized KdV equation. In Chapter 2 and Chapter 3, we introduce the following artificial bound-

aries:

$$\begin{aligned}\Omega_a &= \{(x,t)|x=a,\ 0\le t\le T\},\\ \Omega_b &= \{(x,t)|x=b,\ 0\le t\le T\}.\end{aligned}$$

and based on the artificial boundaries, we manage to divide the linear part into 3 subproblems. Before taken inverse Laplace transformation, the exact boundary conditions can be derived as

$$\hat{u}(b,s)-\frac{1}{\lambda_1^2(s)}\hat{u}_{xx}(b,s) = 0, \tag{4.9}$$

$$\hat{u}_x(b,s)-\frac{1}{\lambda_1(s)}\hat{u}_{xx}(b,s) = 0, \tag{4.10}$$

$$\hat{u}(a,s)+\frac{1}{\lambda_1(s)}\hat{u}_x(a,s)+\frac{1}{\lambda_1^2(s)}\hat{u}_{xx}(a,s) = 0. \tag{4.11}$$

The selection of different approximations to $\lambda_1(s)$ and $\lambda_1^2(s)$ leads to varies local absorbing boundary conditions. As a successive work to previous chapters, we use the continued fraction method to design the nonlinear local ABCs.

4.2.2 LABCs for nonlinear KdV equation

The definition of auxiliary variables stays the same as in the Chapter 3 Section 3.3.

$$\lambda_1(s)=-\sqrt[3]{s}=-(1+B_1),\quad \text{with}\quad B_i=\frac{s-1}{f_i+B_{i+1}}, i=1,2,\ldots,p$$

$$\lambda_1^2(s)=\sqrt[3]{s^2}=1+C_1,\quad \text{with}\quad C_i=\frac{s-1}{g_i+C_{i+1}}, i=1,2,\ldots,p$$

- **One-variable case**

  For simplicity, we take $p=1$, then the local ABCs for the linear subproblem

can be formed as

$$\begin{aligned} u_x + u + w_1 &= 0 \\ f_1 w_1 &= u_t - u \\ u_{xx} - u - v_1 &= 0 \\ g_1 v_1 &= u_t - u \\ u_{xx} - u_x + u - \bar{v}_1 + \bar{w}_1 &= 0 \\ f_1 \bar{v}_1 &= u_{xt} - u_x \\ g_1 \bar{w}_1 &= u_t - u \end{aligned}$$

that is,

$$\frac{1}{f_1} u_t = [-\frac{\partial}{\partial x} + (\frac{1}{f_1} - 1)]u \tag{4.12}$$

$$\frac{1}{g_1} u_t = [\frac{\partial^2}{\partial x^2} + (\frac{1}{g_1} - 1)]u \tag{4.13}$$

$$[\frac{1}{f_1}\frac{\partial}{\partial x} - \frac{1}{g_1}]u_t = [\frac{\partial^2}{\partial x^2} + (\frac{1}{f_1} - 1)\frac{\partial}{\partial x} + (1 - \frac{1}{g_1})]u \tag{4.14}$$

For simplicity, let's denote $[\frac{1}{f_1}\frac{\partial}{\partial x} - \frac{1}{g_1}]$ with an operator $\mathbf{W}$, then on the right boundary, Eq. (4.12)-(4.14) become

$$u_t = [-f_1\frac{\partial}{\partial x} + (1 - f_1)]u := \hat{\mathbf{L}}_1 u \tag{4.15}$$

$$u_t = [g_1\frac{\partial^2}{\partial x^2} + (1 - g_1)]u := \hat{\mathbf{L}}_2 u \tag{4.16}$$

$$u_t = \mathbf{W}^{-1}[\frac{\partial^2}{\partial x^2} + (\frac{1}{f_1} - 1)\frac{\partial}{\partial x} + (1 - \frac{1}{g_1})]u := \hat{\mathbf{L}}_3 u \tag{4.17}$$

Up to this point, in Eq. (4.15)-(4.17) we obtain the approximated linear operator on the artificial boundaries, i.e. $\hat{\mathbf{L}}_1, \hat{\mathbf{L}}_2$ for the right boundary and $\hat{\mathbf{L}}_3$ for the left one. Apply the approximated linear operators on KdV equation and we will deduce three local absorbing boundary conditions for nonlinear equation,

given as Eq. (4.18)-(4.20)

$$u_t = [-f_1\frac{\partial}{\partial x} + (1-f_1)]u + \mathbf{N}u \tag{4.18}$$

$$u_t = [g_1\frac{\partial^2}{\partial x^2} + (1-g_1)]u + \mathbf{N}u \tag{4.19}$$

$$u_t = \mathbf{W}^{-1}[\frac{\partial^2}{\partial x^2} + (\frac{1}{f_1}-1)\frac{\partial}{\partial x} + (1-\frac{1}{g_1})]u + \mathbf{N}u \tag{4.20}$$

- **Two-variable case**

  Choose $p = 2$ for continued fraction approximation. When on the right boundaries, we have

$$u_x + u + w_1 = 0 \tag{4.21}$$

$$f_1 w_1 + w_2 = u_t - u \tag{4.22}$$

$$f_2 w_2 = w_{1,t} - w_1 \tag{4.23}$$

$$u_{xx} - u - v_1 = 0 \tag{4.24}$$

$$g_1 v_1 + v_2 = u_t - u \tag{4.25}$$

$$g_2 v_2 = v_{1,t} - v_1 \tag{4.26}$$

  With canceling w_i, v_i, $w_{1,t}$ and $v_{1,t}$ out, Eq. (4.21)-(4.26) is deduced as

$$u_{xt} + (f_2+1)u_t = f_2 u + (1-f_1 f_2)(u_x + u) \tag{4.27}$$

$$-u_{xxt} + (g_2+1)u_t = (g_1 g_2 - 1)u_{xx} + (1 - g_1 g_2 + g_2)u \tag{4.28}$$

  On the left boundary,

$$u_{xx} - u_x + u - \bar{v}_1 + \bar{w}_1 = 0 \tag{4.29}$$

$$f_1\bar{v}_1 + \bar{v}_2 = u_{xt} - u_x \tag{4.30}$$

$$f_2\bar{v}_2 = \bar{v}_{1,t} - \bar{v}_1 \tag{4.31}$$

$$g_1\bar{w}_1 + \bar{w}_2 = u_t - u \tag{4.32}$$

$$g_2\bar{w}_2 = \bar{w}_{1,t} - \bar{w}_1 \tag{4.33}$$

Similar procedures have been done on the left boundary. With Eq. (4.29)-(4.33), we rewrite $\bar{v}_1$, $\bar{v}_2$, $\bar{w}_2$, $\bar{w}_{1,t}$ in the equations of u and $\bar{w}_1$, namely

$$\begin{aligned}
\bar{v}_1 &= u_{xx} - u_x + u + \bar{w}_1 && (4.34)\\
\bar{v}_2 &= -f_1\bar{v}_1 + u_{xt} - u_x && (4.35)\\
\bar{w}_2 &= -g_1\bar{w}_1 + u_t + u && (4.36)\\
\bar{w}_{1,t} &= (1 - g_1g_2)\bar{w}_1 + g_2(u_t - u) && (4.37)
\end{aligned}$$

$$\begin{aligned}
u_{xxt} - (1 + f_2)u_{xt} + (1 + g_2)u_t &= (1 - f_1f_2)u_{xx} + (f_1f_2 - f_2 - 1)u_x \\
&\quad +(1 + g_2 - f_1f_2)u + (g_1g_2 - f_1f_2)\bar{w}_1 \quad (4.38)
\end{aligned}$$

However, different from right boundaries, we still lack one equation to cancel out $\bar{w}_1$ in Eq. (4.38), then we solve Eq. (4.37) as an ODE of $\bar{w}_1$,i.e.,

$$\begin{aligned}
\bar{w}_{1,t} + (g_1g_2 - 1)\bar{w}_1 &= g_2(u_t - u) && (4.39)\\
\frac{d}{dt}[e^{(g_1g_2-1)t}\bar{w}_1] &= e^{(g_1g_2-1)t}g_2(u_t - u) && (4.40)\\
\bar{w}_1 &= e^{-(g_1g_2-1)t}\int e^{(g_1g_2-1)s}g_2(u_s - u)ds && (4.41)
\end{aligned}$$

Substitute $\bar{w}_1$ back to (4.38) and we have the left boundary solved as

$$\begin{aligned}
&[-\frac{\partial^5}{\partial x^5} + (1 + f_2)\frac{\partial^4}{\partial x^4} - (1 + g_2)\frac{\partial^3}{\partial x^3} + (g_1g_2 + f_1f_2 - 2)\frac{\partial^2}{\partial x^2} + \dots \\
&(2 + 2f_2 - f_1f_2 - g_1g_2 - g_1g_2f_2)\frac{\partial}{\partial x} + (f_1f_2g_2 + g_1g_2 + f_1f_2 - 2g_2 - 2)] \\
&= (g_1g_2 - 1)(1 - f_1f_2)u_{xx} + (g_1g_2 - 1)(f_1f_2 - f_2 - 1)u_x \\
&\quad + (-f_1f_2g_1g_2 + f_1f_2g_2 + f_1f_2 + g_1g_2 - g_2 - 1)u \quad (4.42)
\end{aligned}$$

For simplicity, let's mark three operators $\mathbf{E}_1, \mathbf{E}_2$ and $\tilde{\mathbf{W}}$ as following

$$[\frac{\partial}{\partial x} + (1 + f_2)] = \mathbf{E}_1,$$

$$[-\frac{\partial^2}{\partial x^2} + (1 + g_2)] = \mathbf{E}_2,$$

$$[-\frac{\partial^5}{\partial x^5} + (1 + f_2)\frac{\partial^4}{\partial x^4} - (1 + g_2)\frac{\partial^3}{\partial x^3} + (g_1g_2 + f_1f_2 - 2)\frac{\partial^2}{\partial x^2} + \dots$$

$$(2+2f_2-f_1f_2-g_1g_2-g_1g_2f_2)\frac{\partial}{\partial x}+(f_1f_2g_2+g_1g_2+f_1f_2-2g_2-2)]=\mathbf{W}.$$

Therefore, we construct three absorbing boundary conditions for linearized KdV equations as:

$$\begin{aligned}
\mathbf{E}_1\frac{\partial u}{\partial t} &= [(1-f_1f_2)\frac{\partial}{\partial x}+(1+f_2-f_1f_2)]u && (4.43)\\
\mathbf{E}_2\frac{\partial u}{\partial t} &= [(g_1g_2-1)\frac{\partial^2}{\partial x^2}+(1+g_2-g_1g_2)]u && (4.44)\\
\tilde{\mathbf{W}}\frac{\partial u}{\partial t} &= [(g_1g_2-1)(1-f_1f_2)\frac{\partial^2}{\partial x^2}+(g_1g_2-1)(f_1f_2-f_2-1)\frac{\partial}{\partial x}\\
&\quad +(f_1f_2-1)(-g_1g_2+g_2+1)]u && (4.45)
\end{aligned}$$

Since we have deduced three boundary conditions for the linear case and we can approximate the linear operator on both east and west boundaries as:

$$\begin{aligned}
\tilde{\mathbf{L}}_1u &:= \mathbf{E}_1^{-1}[(1-f_1f_2)\frac{\partial}{\partial x}+(1+f_2-f_1f_2)]u && (4.46)\\
\tilde{\mathbf{L}}_2u &:= \mathbf{E}_2^{-1}[(g_1g_2-1)\frac{\partial^2}{\partial x^2}+(1+g_2-g_1g_2)]u && (4.47)\\
\tilde{\mathbf{L}}_3u &:= \mathbf{W}^{-1}[(g_1g_2-1)(1-f_1f_2)\frac{\partial^2}{\partial x^2}+(g_1g_2-1)(f_1f_2-f_2-1)\frac{\partial}{\partial x}\\
&\quad +(f_1f_2-1)(-g_1g_2+g_2+1)]u && (4.48)
\end{aligned}$$

Local absorbing boundary conditions for nonlinear cases can be deduced as

$$\begin{aligned}
\frac{\partial u}{\partial t} &= \tilde{\mathbf{L}}_1u+\mathbf{N}u && (4.49)\\
\frac{\partial u}{\partial t} &= \tilde{\mathbf{L}}_2u+\mathbf{N}u && (4.50)\\
\frac{\partial u}{\partial t} &= \tilde{\mathbf{L}}_3u+\mathbf{N}u && (4.51)
\end{aligned}$$

4.3 Numerical results

In this section, we test the effectiveness of our simplest local ABCs for nonlinear KdV equation on finite domain $[a,b]$ with single parameter. Namely, utilize the local absorbing boundary conditions eq. (4.18)-(4.20).

Example 1. We consider the following standard KdV problem

$$\begin{aligned} u_t + u_{xxx} + 6uu_x &= 0, \qquad x \in \mathbb{R}, \\ u(x,0) &= 2\text{sech}^2(x),\ x \in \mathbb{R}, \\ u &\to 0, \qquad x \to \infty. \end{aligned}$$

The analytical solution of this KdV equation is

$$u(x,t) = \frac{1}{2}c \cdot \text{sech}^2[\frac{\sqrt{c}}{2}(x - ct)],$$

This is a right moving soliton, being of a fixed wave form with a phase speed c. In this example, we choose $c = 4$. After coupling with the local ABCs (4.18)-(4.20) and restricted on a bounded domain, the original problem becomes a reduced IBV problem on a finite interval $[a, b]$,

$$u_t + u_{xxx} + 6uu_x = 0, \tag{4.52}$$

$$u_t(b,t) = [-f_1\frac{\partial}{\partial x} + (1 - f_1)]u(b,t) + \mathbf{N}u(b,t), \tag{4.53}$$

$$u_t(b,t) = [g_1\frac{\partial^2}{\partial x^2} + (1 - g_1)]u(b,t) + \mathbf{N}u(b,t), \tag{4.54}$$

$$u_t(a,t) = \mathbf{W}^{-1}[\frac{\partial^2}{\partial x^2} + (\frac{1}{f_1} - 1)\frac{\partial}{\partial x} + (1 - \frac{1}{g_1})]u(a,t) + \mathbf{N}u(a,t), \tag{4.55}$$

$$u(x,0) = 2\text{sech}^2(x). \tag{4.56}$$

where $x \in [a, b], t > 0$.

For given two positive integers J and N, we get the spatial and temporal mesh sizes by defining

$$\Delta x = \frac{b-a}{J}, \Delta t = \frac{T}{N}.$$

Thus, the uniform grid points can be written as

$$x_j = a + j\Delta x, j = 0, 1, 2, \cdots, J$$

and

$$t_n = n\Delta t, n = 0, 1, \cdots, N.$$

u_j^n presents the approximation of $u(x_j, t_n)$. We define the finite difference operators as

$$f_j^{n+1/2} = \frac{f_j^{n+1} + f_j^n}{2}, \quad \delta_t^+ f_j^n = \frac{f_j^{n+1} - f_j^n}{\Delta t}.$$

We adopt the standard Crank-Nicolson finite difference method on the KdV equation in the interior domain:

$$\delta_t^+ u_j^n + \delta_x^3 u_j^{n+1/2} - 3\delta_x (u_j^{n+1/2})^2 = 0,$$

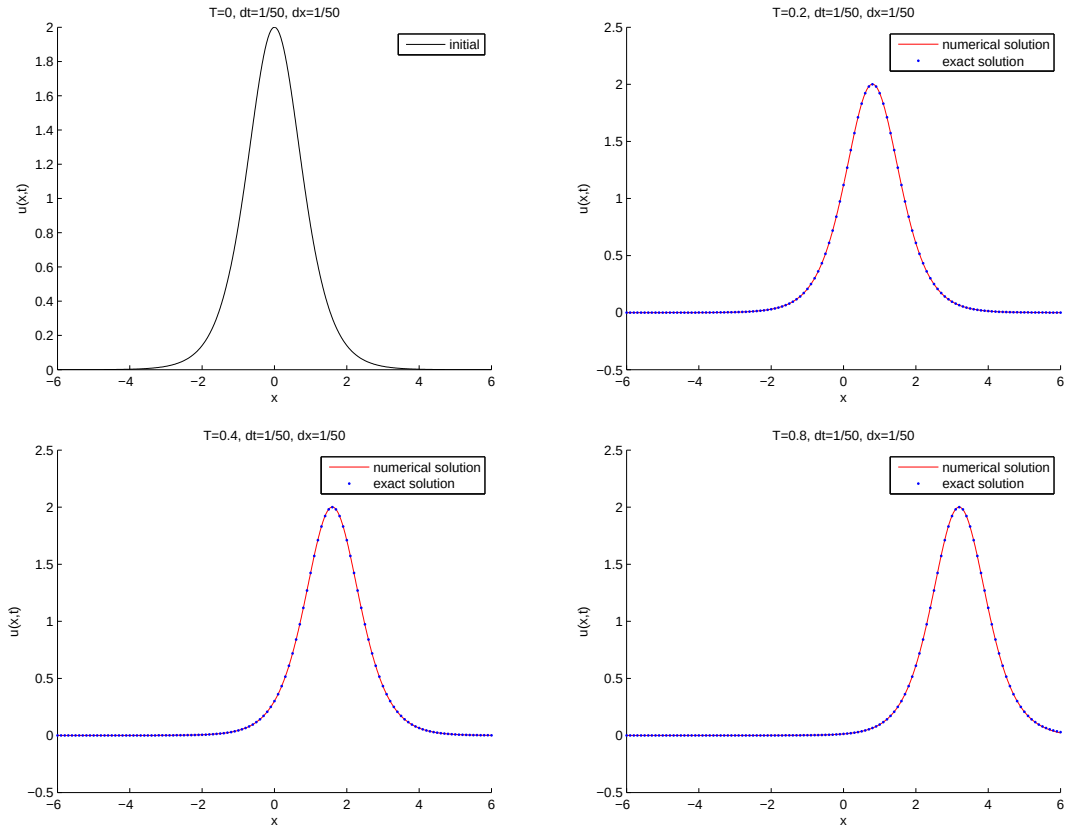

Figure 4.1: Numerical solutions compared with exact solutions at different times with single parameter.

As seen in Fig. 4.1, the local absorbing boundary conditions with single continued fraction parameter for the Korteweg-de Vries equation perform decently at different time. In Fig. 4.2, we present the numerical errors of different time when the numerical

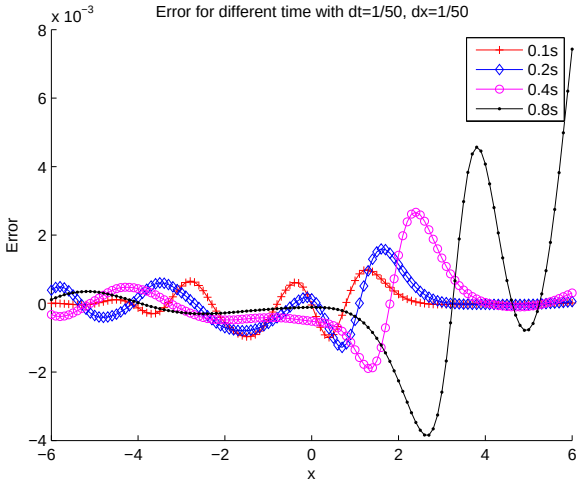

Figure 4.2: Numerical errors compared with exact solutions at different times with single parameter.

solutions fitting the analytic ones. The test results show the obvious advantage of our proposed method with single variable.

Chapter 5

Summary

5.1 Summary of the thesis

In this thesis, we have designed several local absorbing boundary conditions for both the linearized KdV equation and the nonlinear KdV equation. In Chapter 2, accurate local absorbing boundary conditions for a linearized KdV equation is proposed. The reason why we adopt the Padé approximation in the first place, is because of the accuracy and efficiency of its performance. More importantly, the Padé approximation allows us to directly obtain the local absorbing boundary conditions through inverse Laplace transformation. The test results about the accuracy and efficiency of the Padé approximation to the target function turn out that when p is greater than 5, the estimation to is good enough for further use. We then construct the local ABCs with Padé approximation. Applying the absorbing boundary conditions, we yield a reduced initial boundary value problem defined on a finite domain. The accuracy of the inverse Laplace transformation on the approximation to the cubic root is tested numerically in Chapter 2 Section 2.3, followed by the stability of the reduced initial boundary value problem. Then the local ABCs with Padé approximation are implemented by the finite difference method. We provide two numerical examples in supporting our theory. The numerical results are presented to demonstrate the stability and accuracy of the proposed method. One can achieve high accuracy even with a small parameter p.

We also provide another approach, the continued fraction method, to estimating the cubic root. Inspired by Guddati and Tassoulas[15], we provide a continued

fraction approximation of the cubic root function and obtain three local ABCs for the linearized KdV model to surpass the expensive computational cost introduced by the convolution operations. The other advantages of the continued fraction method include the good form of the parameters which allow us to have further extension on the nonlinear model. The performance of the local ABCs with continued fraction method is also tested in Chapter 3.

In general, the Padé approximation and continued fraction approximation are two different approaches in every aspect, and there are advantages and shortages in both methods. The Padé method provides accurate approximation for local ABCs even with small amount of parameters. However, due to the imperfection of the nonlinear system for solving Padé coefficients, the reduced problem with local ABCs suffers from fluctuations while p too large. On the other hand, for the continued fraction method, the explicit formula for continued fraction coefficients can be derived, which will be useful for further research on stability analysis for both linearized and nonlinear KdV equations. Compared to the Padé approximation, the continued fraction approximation requires larger amount of parameters to achieve the same level of accuracy.

Based on the work we done on the linearized KdV model with continued fraction method, we propose split local absorbing boundary conditions with the continued fraction by introducing the unifying approach method and manage to extend the research to nonlinear Korteweg-de Vries equation. The idea of the unifying approach method is to separate inward- and outward-going waves and to build suitable approximated linear operator with a "one-way operator". Uniting the approximated linear operator with the nonlinear subproblem, we may propose the corresponding boundary conditions for the reduced nonlinear problem along the artificial boundaries. For simplicity, we only adopt small amount of auxiliary variables. The local ABCs for nonlinear KdV with single/double parameters are deduced in Chapter 4. The numerical test results shows the good behavior of the nonlinear local ABCs with

single parameter.

5.2 Future research

Future research directions will include the improvement of the accuracy and efficiency of the local ABCs, the numerical stability of the linearized KdV equation with both approaches. The second direction of research would be to design the local ABCs for the multi-dimensional KdV equation and other KdV-type equations on unbounded domain.

Bibliography

[1] G. B. Witham, *Linear and nonlinear waves* (Wiley, New York, 1974).

[2] R. K. Dodd, J. C. Eilbeck, J. D. Gibbon, H. C. Morris, *solitons and nonlinear wave equations* (Academic Press, London, 1982).

[3] C. Zheng, X. Wen, H. Han, Numer. Meth. PDEs 24, 383 (2006).

[4] H. Han, X. Wu, *Artificial boundary method* (Spring-Verlag and Tsinghua University Press, Berlin Heidelberg and Beijing, 2013).

[5] C. Zheng, Numer. Math. 105, 315 (2006).

[6] E. L. Lindman, J. Comput. Phys. 18, 66 (1975).

[7] B. Engquist, A. Majda, Math. Comput. 31, 629 (1977).

[8] T. Hagstrom, M. Castro, D. Givoli, D. Tsemach, J. Comput. Acoust. 15, 1 (2007).

[9] T. Hagstrom, A. Mar-Or, D. Givoli, J. Comput. Phys. 227, 3322 (2008).

[10] T. Hagstrom, T. Warburton, Wave Motion 39, 327 (2004).

[11] T. Hagstrom, T. Warburton, SIAM J. Numer. Anal. 47(5), 3678 (2009).

[12] E. Bécache, D. Givoli, T. Hagstrom, J. Comput. Phys. 229, 1099 (2010).

[13] T. Hagstrom, H.B. Keller, Math Comput. 48, 449, (1987).

[14] A.J. Safjan, Comput. Meth. Appl. Mech. Engng., 152, 175C193, (1998).

[15] M. N. Guddati, J. L. Tassoulas, J. Comput. Acoust. 8, 139 (2000).

[16] X. Wu, J. Zhang, J. Comput. Math. 29, 74 (2011).

[17] J. Zhang, Z. Xu, X. Wu, Phys. Rev. E 78, 026709 (2008).

[18] J. Zhang, Z. Xu, X. Wu, Phys. Rev. E 79, 046711 (2009).

[19] H. Brunner, X. Wu, J. Zhang, SIAM J. Sci. Comput. 6, 4478 (2010).

[20] J. Zhang, H. Han, H. Brunner, J. Sci. Comput. 49, 367 (2011).

[21] A. Arnold, M. Ehrhardt, M. Schulte, I. Sofronov, Commun. Math. Sci. 10(3), 889 (2012).

[22] E.F.G. van Daalen, J. Broeze, E. van Groesen, Math. Comput. 58(197), 55 (1992).

[23] J. Broeze, E.F.G. van Daalen, Math. Comput. 58, 73 (1992).

[24] Z. Xu, H. Han, X. Wu, Commun. Comput. Phys. 1, 479 (2006).

[25] H. Han, X. Wu, Z. Xu, J. Comput. Math, 24, 295, (2006).

[26] J. Zhang, Z. Z. Sun, X. Wu, D. Wang, Commun. Comput. Phys. 10(3), 742 (2011).

[27] Z. Xu, H. Han, Phys. Rev. E, 74, 037704, (2006).

[28] Z. Xu, H. Han, X. Wu, J. Comput. Phys. 225, 1577 (2007).

[29] X. Antoine, C. Besse, P. Klein, SIAM J. Sci. Comput. 33(2), 1008 (2011).

[30] H. Li, X. Wu, J. Zhang, Phys. Rev. E, 84, 036707 (2011).

[31] H. Han, Z. W. Zhang, Commun. Comput. Phys. 10(5), 1161 (2011).

[32] X. Antoine, A. Arnold, C. Besse, M. Ehrhardt, and A. Schädle, Commun. Comput. Phys. 4(4), 729 (2008).

[33] C.-H. Bruneau, L. Di Menza, T. Lehner, Numer. Meth. Part. Diff. Eq., 15, 672 (1999).

[34] J. Szeftel, SIAM J. Numer. Anal., 42, 1527 (2004).

[35] J. Szeftel, Math. Comput., 75, 565 (2006).

[36] T. Fevens, H. Jiang, SIAM J. Sci. Comput., 21(1), 255 (1999).

[37] R. Gorenflo, F. Mainardi, *Fractional calculus: integral and differential equations of fractional order, in: A. Carpinteri, F. Mainardi (Eds.), Fractals and Fractional Calculus in Continuum Mechanics* (Springer, Wien, 1997).

[38] Korteweg D. J., de Vries F., Philos. Mag. 39, 422-443 (1895).

[39] Boussinesq J., Memoires presentes par divers savants ‘ lAcad. des Sci. Inst. Nat. France, XXIII, pp.1C680, (1877).

[40] Zabusky N. J., Kruskal M. D., Phys. Rev. Lett, 15(6), 240-243, (1965).

[41] Gardner C. S., Greene J. M., Kruskal M. D. and Miura R. M., Phys. Rev. Lett., 19(19), 1095–1097, (1967).

[42] Miura R. M., J. Math. Phys. 9, 1202-1204, (1968).

[43] Miura R. M., Gardner C. S., and Kruskal M. D., J. Math. Phys. 9, 1204-1209, (1968).

[44] Lax P. D., Communications on Pure & Applied Mathematics, 21(5), 467-490, (1968).

[45] Taha T R, Ablowitz M I., Journal of Comput. Phys., 55(2), 231-253, (1984).

[46] Fokas A.S., Comm. Pure Appl. Math., 58(5), 639-670, (2005).

[47] Berenger J. P., Journal of Comput. Phys., 114(2), 185-200., (1994).

[48] Wrobel L. C., Aliabadi M. H.,*The Boundary Element Method*(New York: John Wiley & Sons, p. 1066, 2002).

[49] R. K. Dodd, J. C. Eilbeck, J. D. Gibbon, and H. C. Morris, *Solitons and nonlinear wave equations* (Academic Press, London, 1982).

[50] Ablowitz M. J., Segur H., *Solitons and the inverse scattering transform[M]* (Philadelphia: Siam, 1981).

[51] Winther R., Mathematics of Computation, 23-43, (1980).

[52] K. Goda , J. Phys. Soc. Japan, 39, 229-236, (1975).

[53] Gardner C. S., Morikawa G. K., *Similarity in the Asymptotic Behavior of Collision-Free Hydromagnetic Waves and Water Waves* ("New York Univ., Courant Inst. Math. Sci" Res. Report, NYO-9082, 1960).

[54] J. Shen, SIAM J. Numer. Anal., 41, 1595C1619, (2003).

[55] Strang G., SIAM J. Numer. Anal., 5(3), 506-517, (1968).

[56] L. A. Khan and P. L. F. Liu, Comput. Methods Appl. Mech. Eng. 152, 337 (1998).

CURRICULUM VITAE

Academic qualifications of the thesis author, Ms. ZHANG Wei:

- Received the degree of Bachelor of Science (Honors) from Hong Kong Baptist University, July 2010.
- Received the degree of Master of Science (Operation Research and Business Statistics) from Hong Kong Baptist University, August 2011.

Published Papers

- W.Zhang, H. Li, X. Wu, *Local absorbing boundary conditions for a linearized Korteweg-de Vries equation*, Phys. Rev. E, 2014, 89(5): 053305.

Conference Presentation

- The 9th East Asia SIAM Conference, Indonesia June 23-26, 2014

  Presentation title: Local Absorbing Boundary Conditions for a Linearized Korteweg-de Vries Equation on Unbounded Domains.

September 2014